1985

Geology of the Idol City area: A volcanic-hosted disseminated precious-metal occurrence in east-central Oregon

Daniel J. McGrane
The University of Montana

GEOLOGY OF THE IDOL CITY AREA: A

VOLCANIC-HOSTED, DISSEMINATED, PRECIOUS-METAL

OCCURRENCE IN EAST-CENTRAL OREGON

by   .

Daniel J. McGrane

B.S., Colorado State University, 1979

Presented in partial fulfillment of the
requirements for the degree of

Master of Science

UNIVERSITY OF MONTANA

1985

Approved by:

Chairman, Board of Examiners

Dean, Graduate School

Date

UMI Number: EP38337

UMI[•]

Dissertation Publishing

UMI EP38337

ProQuest[•]

ABSTRACT

McGrane, Daniel J., M.S., Spring 1985   Geology

Geology of the Idol City Area: A Volcanic-Hosted, Disseminated,
Precious-Metal Occurrence in East-Central Oregon (88 pp.)

Director: Ian M. Lange 〴〵.

The Idol City area is 32 kilometers northeast of Burns, in
Harney County, Oregon. The property is underlain by a thick
sequence of early Miocene lavas of intermediate composition.
These lavas were intruded by several porphyritic rhyolite dikes
and plugs, and coarser-grained quartz-porphyry granitic bodies.
Intrusive and extrusive rocks are exposed along the crest of a
regional south-plunging anticline and are flanked by younger
ash-flow tuffs. Base- and precious-metal mineralization is
confined to andesitic rocks which are sheared, brecciated, and
hydrothermally altered.

Previous studies viewed mineralization at Idol City as typical
of the upper part of a vein-type hydrothermal system. This study
shows that base and precious metals occur primarily as dissemin-
ations and filling stockworks within two broad tourmalinized
breccia zones which formed during explosive hydrothermal activity.
Mineralization within these zones is remarkably consistent over
broad vertical and lateral distances.

Deposition of metals occurred in response to boiling triggered
by episodic explosive brecciation events. Boiling temperatures of
approximately $300°C$, determined from fluid inclusion studies on
mineralized stockworks, indicate that metal deposition could have
occurred at depths as shallow as 315 meters. Felsic intrusive
bodies are spatially, temporally, and probably genetically related
to the mineralizing event.

ACKNOWLEDGEMENTS

TABLE OF CONTENTS

TABLE OF CONTENTS
(continued)

LIST OF FIGURES

LIST OF FIGURES
(continued)

Figure

LIST OF TABLES

LIST OF PLATES

Plate

INTRODUCTION

Having limited the source of most placer gold to a small drainage basin above the Idol City townsite, old-timers concentrated their efforts on locating the mother-lode. Hundreds of pits, trenches, adits, and shafts were dug adjacent to the Gold Gulch drainage. Although most rocks yielded minor amounts of gold, high-grade zones were never located.

Recently, this broad distribution of anomalous gold was recognized by Noranda Exploration, Inc. geologists. Early studies by Noranda in 1980 and 1981 were sample intensive and workers assumed the Idol City system represented the upper part of a typical vein-type deposit. However, preliminary investigation of the area by myself in 1982 indicated that alteration and mineralization were centered about two zones of intense fracturing and brecciation exhibiting characteristics of a disseminated precious-metal system. These zones became the target of future exploration activity by Noranda and the focal point of my study.

The following study establishes a genetic interpretation for mineralization. Genetic relationships of ore to host lithologies, structures, alteration, and igneous activity were examined. This information will contribute to the knowledge and understanding of disseminated precious-metal systems.

Methods of Investigation

Detailed surface mapping and logging of drill-hole cuttings and core aided in constructing stratigraphic, structural, and intrusive relationships. Petrography and whole-rock chemistry complimented geologic mapping, especially in areas subjected to hydrothermal alteration. X-ray diffraction, fluid inclusion, and trace element geochemical analyses assisted in identifying the character and effects of hydrothermal fluids. Two K-Ar age determinations established the temporal relationship between intrusive activity and the mineralizing event.

Location and Access

The Idol City area is 32 kilometers northeast of Burns, in Harney County, Oregon (Figure 1). The property is named after the old townsite of Idol City, recognized now by the presence of a few run-down cabins at the confluence of Trout Creek and Gold Gulch (Figure 2). Access from Burns is via U.S. Highway 395 and improved Forest Service gravel roads. The topography is relatively subdued with elevations ranging from 1800 to 2100 meters above sea level.

Previous Studies

No detailed, published geologic studies of the Idol City area are available. Walker (1979) discussed the regional structure, stratigraphy, and geochronology. Detailed petrographic works by Green
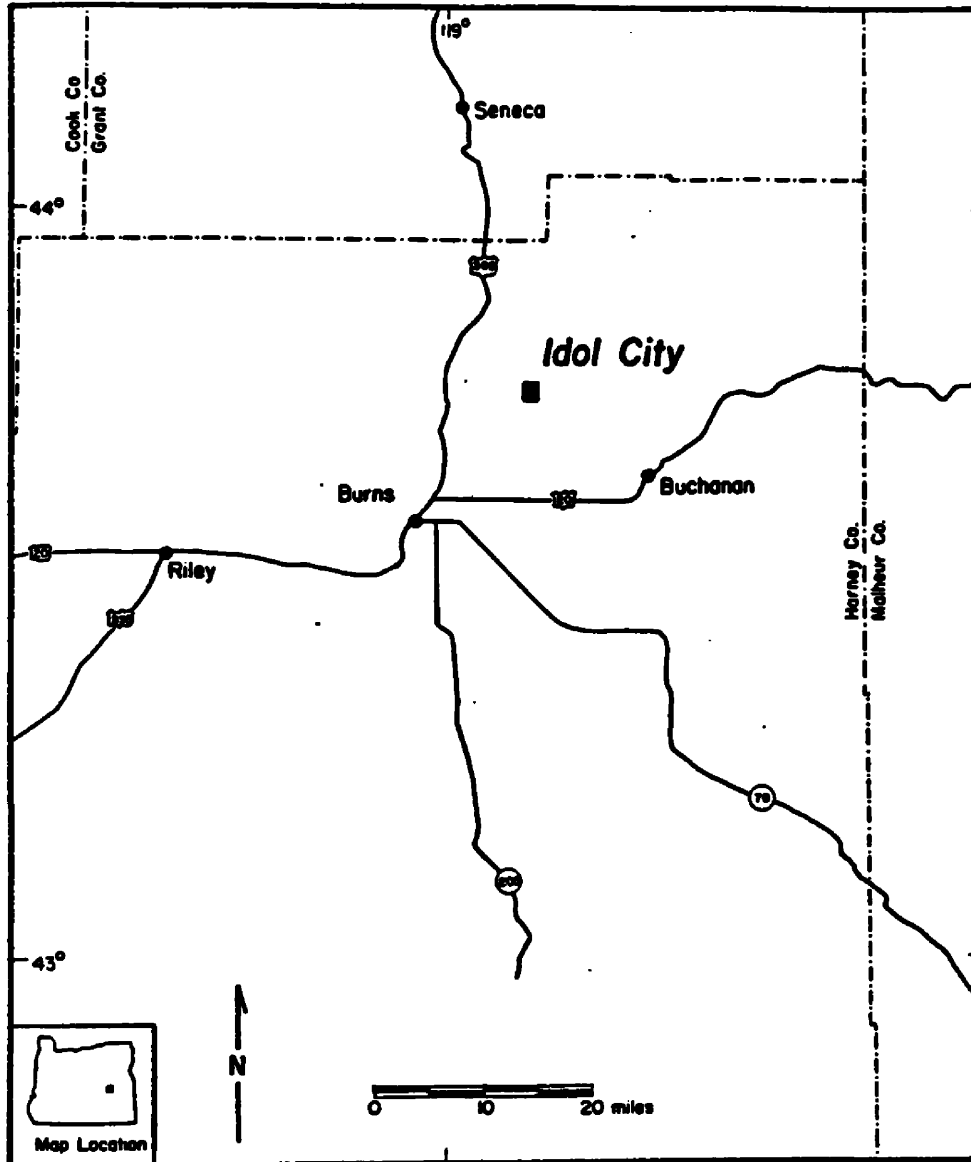
Figure 1: Location map of study area.

Figure 2: Photograph of Idol City and the Gold Gulch
drainage viewed from the north.

(1973) and Enlows (1976) concentrate on volcanic rocks younger than mineralized stratigraphy at Idol City. The only published geologic maps are at scales of 1:250,000 (Green and others, 1972) and 1:500,000 (Walker, 1977).

Parks and Swartley presented the first economic evaluation of Idol City in 1916. Recent geologic and economic accounts are in response to private mineral-exploration programs carried out by Mitchel (1962) and Noranda geologists Davie, Leavitt and Howell (1980), Leavitt (1981), and McGrane (1982,1983, and 1984).

Production History

Approximately 300 people resided at Idol City during the height of placer activity between 1885 and 1900 (Mitchel, 1962). During this time an estimated 2,500 ounces of gold was recovered (Parks and Swartley, 1916).

Shortly after the turn of the century placer miners shifted their attention to hard-rock deposits. In search of the source of placer deposits, prospectors made hundreds of excavations in surrounding areas. Despite these efforts little if any ore was shipped (Martin, personal comm. 1984).

Placering operations were renewed during 1941 when Harry England and Clyde Riddel of Eugene, Oregon mined the lower two thirds of Gold Gulch with a small floating dredge. United States Mint receipts in 1941 indicate recovery of about 17,000 ounces of gold from 200,000 yards of gravel (Mitchel, 1962).

REGIONAL GEOLOGIC AND TECTONIC SETTING

The Idol City prospect is situated in the northeastern part of the High Lava Plains physiographic province (Figure 3); a narrow middle to upper Cenozoic volcanic upland which extends about 250 kilometers eastward from the High Cascages to the east margin of Harney Basin (Walker, 1969a). The province is dominated by a major west-northwest-trending zone of en- echelon normal faults informally designated the Brothers fault zone. This fault system marks the transition between extensional tectonic features of the Basin and Range province to the south and compressional features of the Blue Mountain uplift to the north (Lawrence, 1976).

Uplift and erosion to the north have exposed over 15,000 meters of complexly folded, faulted, and metamorphosed pre-Tertiary sediments, volcanic rocks, and plutonic bodies within 20 kilometers of the study area. Sedimentation, volcanism, and tectonism from late Paleozoic to late Jurassic time reflect deposition under oceanic, probably island arc, conditions. Intrusion of dioritic stocks and batholiths in this region during middle Cretaceous time signaled an abrupt change in sedimentation and represents an early stage of cratonization of the Blue Mountain region following its accretion to the continental margin (Robyn, 1979). Middle Cretaceous continental fluviatile and shallow marine deposits derived from the north were deposited unconformably on older marine strata (Thayer, 1969).
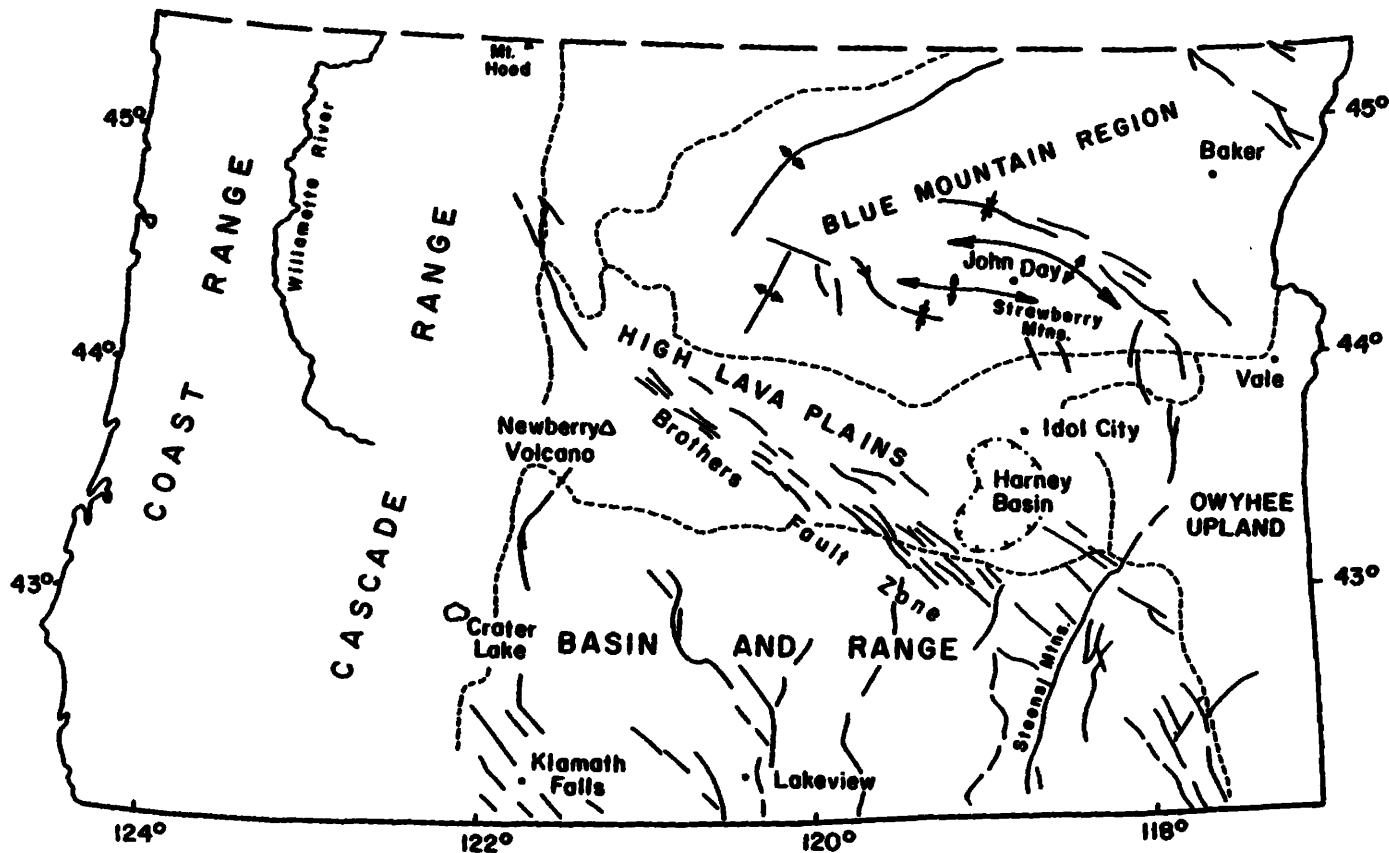
Figure 3 : Index map showing major structural elements of eastern Oregon (modified after Walker, 1977; and Dicken, 1950). The High Lava Plains is dominated by a major zone of en echelon strike-slip faults which separates extensional faulting of the Basin and Range from compressional features of the Blue Mountain Region.

Cenozoic rocks are separated from the older metamorphic and plutonic terrain by a profound regional unconformity. Volcanism began about 41 million years ago with deposition of andesitic lavas, breccias, and tuffaceous sediments of the Clarno Formation (Walker, 1977). Calc-alkaline volcanic rocks of the Clarno Formation are part of a regionally extensive zone of coalescing intermediate- composition volcanic fields which covered much of Washington, Idaho, and western Montana during Eocene time (Lipman and others, 1972). This early Cenozoic volcanism has been related to the evolution of a shallow-dipping imbricate subduction zone under the continental margin from late Cretaceous through Oligocene time (Lipman and others, 1972).

Uplift in the Blue Mountain region, which began about 36 million years ago, resulted in folding, faulting, and erosion of the Clarno Formation prior to deposition of silicic tuffs, flows, and tuffaceous sedimentary rocks over much of central and western Oregon during Oligocene time (Swanson and Robinson, 1968). Silicic volcanic and volcaniclastic rocks north of Idol City have been assigned to the John Day Formation. They are comparable in lithology and possibly age to the Pike Creek and Alvord Creek Formations exposed along the base of the Steens Mountains to the south (Walker, 1969b). Silicic volcanic rocks have a combined thickness of about one thousand meters in uplifted areas to the north and hundreds of meters at the base of the Steens Mountains (Beaulieu, 1972).

In early or middle Miocene time regional extension east of the Cascades marked an abrupt change in the style of volcanism (Christiansen and Lipman, 1972). Early Cenozoic silicic volcanic rocks were blanketed by voluminous basaltic and andesitic lavas which covered most of eastern Oregon to depths commonly exceeding 2,000 meters by late Miocene time. Major coeval eruptive sequences which contributed to this regionally extensive unit include: high alumina basalts of the Steens Mountains and Owyhee regions in the Basin and Range province to the south; and tholeiitic flood basalts of the Columbia River Group to the north (Walker, 1979). The transition between dominantly tholeiitic basalts to the north and high alumina basalts to the south is marked by the presence of a few isolated calc-alkaline volcanic centers. Robyn (1979) suggests these calc-alkaline vents and composite shield volcanoes which occur transverse to contemporaneous andesitic volcanic centers of the western Cascades are not related to subduction, but rather to their unique tectonic setting; the transition between compressional and extensional tectonic regimes.

Approximately ten million years ago volcanism ceased to the north, and renewed uplift raised the Blue Mountains along older, generally east-trending, fold axes (Thayer, 1969). In contrast, the Basin and Range province was experiencing strong east-west extensional faulting and contemporaneous bimodal volcanism which has continued through Recent time. Silicic vents show a progressive decrease in age from Harney Basin (9-10 m.y.) westward to Newberry Volcano (1720 $\pm$250 years old) across apparent northeast-trending isochrons (Macleod and others, 1975).

GEOLOGY OF THE IDOL CITY AREA

The Idol City area lies on the northeast flank of Harney Basin (Figure 4), a structural downwarp which evolved during late Tertiary time (Walker, 1979). Basin subsidence is associated with voluminous eruptions of rhyolite tuff which once extended over 18,000 square kilometers (Greene, 1973).

The property occurs in intermediate-composition lavas which pre-date caldera activity and roughly correlate with the Strawberry volcanic sequence of Brown and Thayer (1966). Intermediate lavas were intruded by several porphyritic rhyolite dikes and plugs, and coarser-grained quartz-porphyry granitic bodies (Plate 1). Intrusive and extrusive rocks are exposed along the crest of a south plunging anticline and are flanked by younger ash-flow tuffs. Relative stratigraphic positions of rock units are illustrated in Figure 5.

The structural fabric is dominated by numerous north- and northwest-trending high-angle shears and faults and two broad northeast-trending zones of intense fracturing and brecciation which became the locus of hydrothermal activity (Plate 2). Chemical and physical conditions associated with hydrothermal activity produced a complex suite of alteration mineral assemblages and resulted in the deposition of base and precious metals over a broad area.
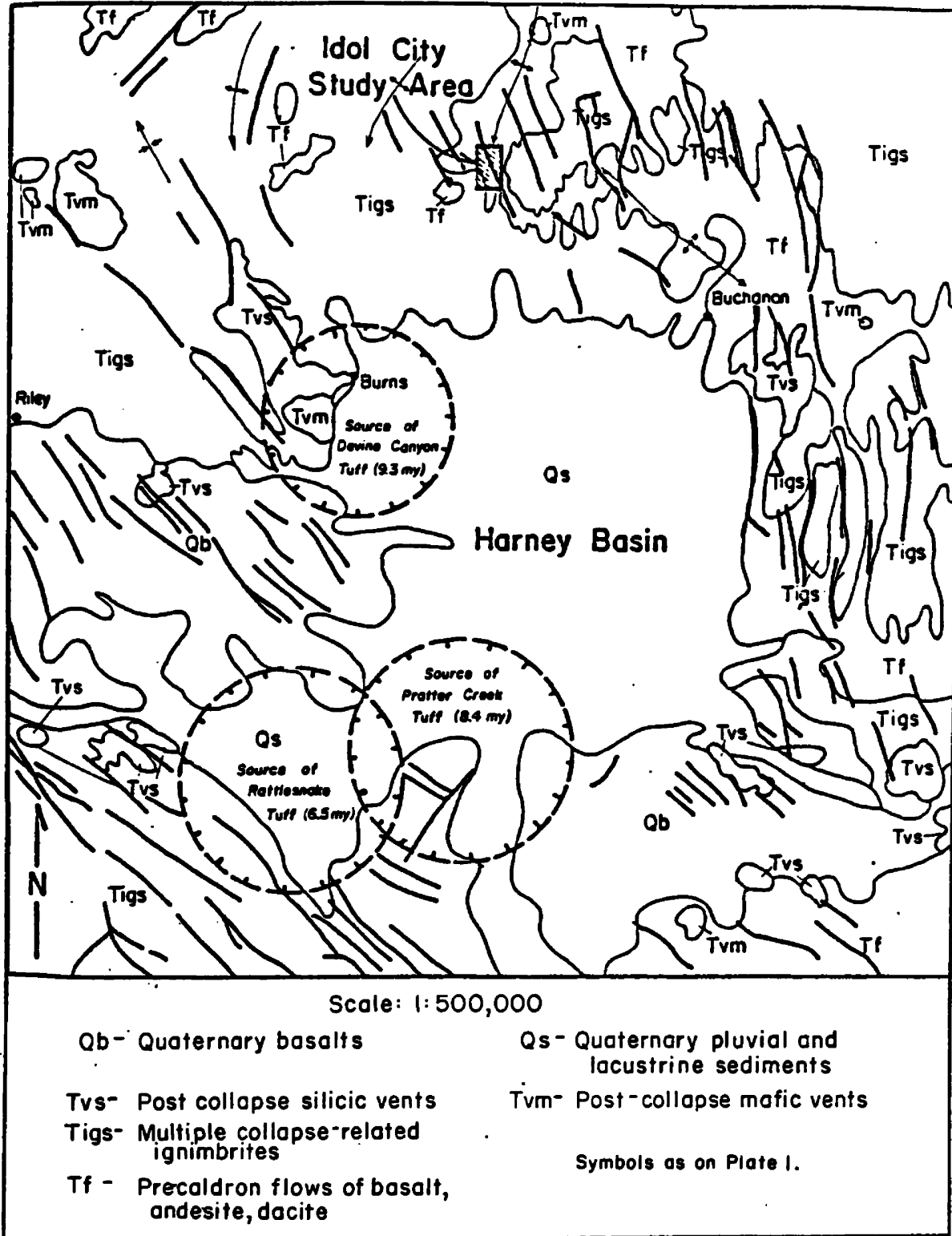
Figure 4: Geologic setting of study area (modified after Walker, 1977 and 1979).
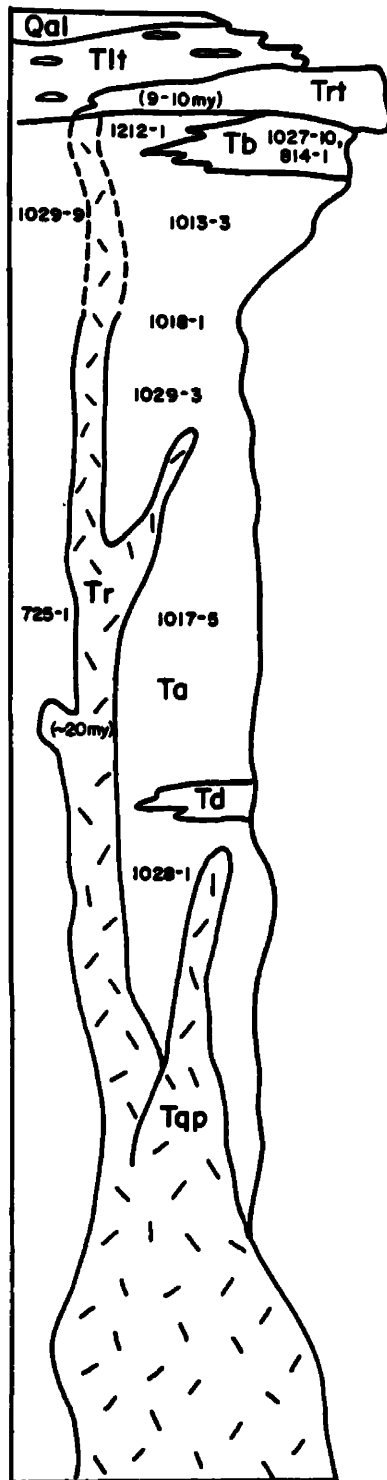
Qal- Alluvium

Tlt - Latite lapilli tuff: contains ≤3% plagioclase and K-feldspar microphenocryst and 15-30% coarse pumice lapilli in a fine vitroclastic groundmass.

Trt - Rhyolite welded tuff: contains 10-15% combined quartz and sanidine phenocrysts and minor sodic pyroxene in a moderate-strongly welded vitroclastic groundmass.

Tr - Rhyolite intrusions: contain 10-15% quartz and sanidine phenocrysts in a white, felty, sericitized and locally silicified aphanatic groundmass.

Tqp- Quartz-porphyry granitic intrusions: porphyritic to hypidiomorphic granular, composed of rounded resorbed quartz and feldspar up to 1cm, local myrolitic cavities.

Tb - Basalt: includes two varieties; Aphyric variety (Tb₁) comprised of dense ophitic growth of plagioclase and augite. Porphyritic variety (Tb₂) contains abundant groundmass olivine.

Td - Dacite: contains 4-5% coarse plagioclase phenocrysts and 3-5% hornblende and biotite microphenocrysts with intergranular quartz, feldspar, and clay.

Ta - Andesites: upper lavas dominantly porphyritic containing 10-25% plagioclase and 4-5% augite and hypersthene phenocrysts. Lower andesites texturally varied, characterized by hornblende as dominant or only mafic phase.

1018-1 -Samples collected for whole rock analysis.

(9-10 m.y.) - Radiometric age determinations.

Figure 5: Generalized stratigraphy of study area showing relative positions of samples collected for whole rock analysis (Table 1). Sample locations are given on Plate 1.

Stratigraphy

Andesites (Ta)

Andesite lavas are the oldest, most widely distributed rock type. These lavas, which show a variety of mineralogies and textures are confined to one map unit due to limited exposure and the effects of hydrothermal alteration. However, stratigraphic relationships of flow units were determined though chemical and petrographic means. Whole rock chemistry of select samples are given in Table 1 and petrographic descriptions are listed in Appendix A.

Andesitic rocks can be divided petrographically into two mineralogically distinct sequences. The lowermost andesite sequence, exposed mainly along the flanks of Gold Gulch in the vicinity of the north breccia zone, is dominated by lavas containing hornblende as the predominant or only mafic phase. Hornblende andesites are capped by a thicker, widely distributed two-pyroxene andesite sequence which is well exposed at higher elevations west and southeast of Gold Gulch. The transition between hornblende and pyroxene andesites is marked by a distinct change in rock composition (Table 1); pyroxene andesites contain more CaO, MgO, and Fe2O3 and less SiO2 than underlying hornblende andesites.

Hornblende andesites rarely crop out and fresh exposures are extremely uncommon. Typically these lava are sparsely porphyritic; plagioclase and hornblende phenocrysts or microphenocrysts constitute 15 percent or less. Phenocrysts are set in a pinkish-grey to black, dense

TABLE 1: Composition of Andesites and Basalts

| | Two Pyroxene Andesites | | | | Hornblende Andesites | | | | Basalts | |
| | Upper | | Lower | | | | | | | |
	1029-9	1013-3	1018-1	1029-3	725-1	1212-1	1017-5	1028-1	814-1	1027-10
SiO_2	61.5	60.9	56.1	56.3	62.8	62.0	60.2	60.4	47.4	47.6
Al_2O_3	16.2	16.9	16.7	16.2	16.4	15.6	15.5	16.4	15.9	15.8
CaO	5.19	5.58	6.35	3.98	4.69	4.83	4.59	4.98	10.9	10.2
MgO	2.76	2.53	3.27	3.86	2.46	1.12	2.33	2.49	6.08	6.51
Na_2O	3.88	3.55	3.74	4.26	4.14	3.95	3.95	3.49	2.71	2.66
K_2O	2.30	2.37	1.96	1.43	2.26	2.39	1.69	1.94	0.52	0.58
Fe_2O_3	5.06	4.78	6.89	6.63	4.95	5.00	5.65	4.78	11.7	12.0
MnO	0.08	0.07	0.11	0.22	0.08	0.11	0.13	0.10	0.18	0.17
TiO_2	0.59	0.73	0.91	0.80	0.61	0.81	0.91	0.62	1.45	1.47
P_2O_5	0.22	0.23	0.28	0.26	0.26	0.31	0.30	0.22	0.22	0.22
Cr_2O_3	<0.01	<0.01	<0.01	<0.01	<0.01	<0.01	<0.01	<0.01	0.02	0.01
H_2O	1.31	1.93	1.47	5.77	0.85	3.62	4.23	4.39	1.54	1.54
Total	99.2	99.7	99.9	99.8	99.6	99.8	99.6	100.1	98.7	98.8
Rb	50	50	50	30	40	50	40	40	<10	20
Sr	740	710	630	550	870	620	710	550	340	270
Zr	120	110	130	130	110	130	170	160	60	70

Major and trace element abundances determined using x-ray fluorescence spectometry by X-Ray Assay Lab, Ltd., Don Mills, Ontario. Stratigraphic positions of samples in Figure 5 and sample locations given on Plate 1.

pilotaxitic or fine-grained intergranular groundmass of plagioclase, mafics, opaque oxides, and minor glass (figure 6). Plagioclase phenocrysts are the most abundant and locally exhibit two episodes of crystallization, with the largest crystals being strongly corroded and resorbed; smaller crystals are fresher and commonly well zoned. Flows locally exhibit aphanitic, coarsely porphyritic, flow banded, or flow breccia textures.

Overlying the hornblende andesite sequence is a thick blanket of pyroxene andesites which can be subdivided into two chemically and petrographically distinct groups. The lower group is characterized by dark grey dense to vesiculated, porphyritic flows which commonly show well developed large blocky jointing. Individual flows generally range from two to 15 meters thick, based on repetition of vesicular zones in drill core.

In thin section, lower pyroxene andesites contain ten to 15 percent plagioclase and four to five percent combined augite and hypersthene phenocrysts. Pyroxene phenocrysts are up to three millimeters in length set in a pilotaxitic to hyalopilitic groundmass of plagioclase, glass, pyroxene, and opaques (figure 7). Other flows in this sequence contain plagioclase and pyroxene phenocrysts in excess of 25 percent. Phenocrysts commonly form coarse glomerocrysts. Plagioclase phenocrysts are commonly zoned and locally resorbed or poikilitic, containing inclusions of hypersthene. The dominant pyroxene phase varies throughout thin sections observed. Flows commonly contain ovoid vesicles measuring up to 1.5 centimeters in diameter. Vesicles are
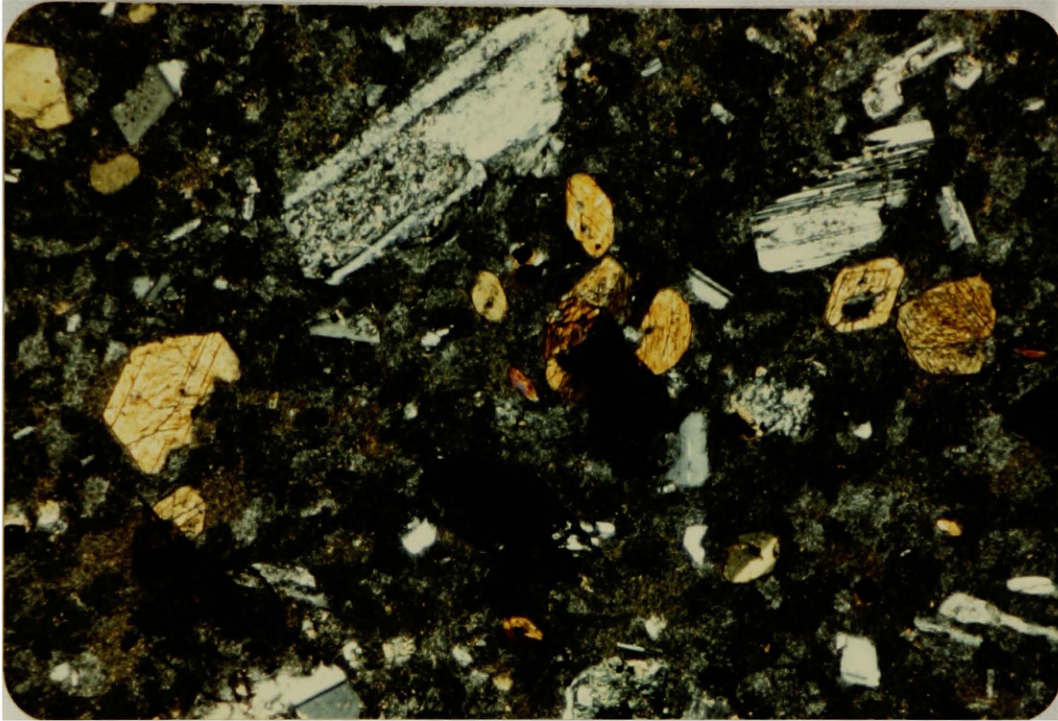
Figure 6 :   Photomicrograph of hornblende andesite comprised
of plagioclase and hornblende microphenocrysts in
a patchy intergranular plagioclase, mafic, and
oxide groundmass.   Cross polars.   Horizontal field
of view approximately 1 cm.
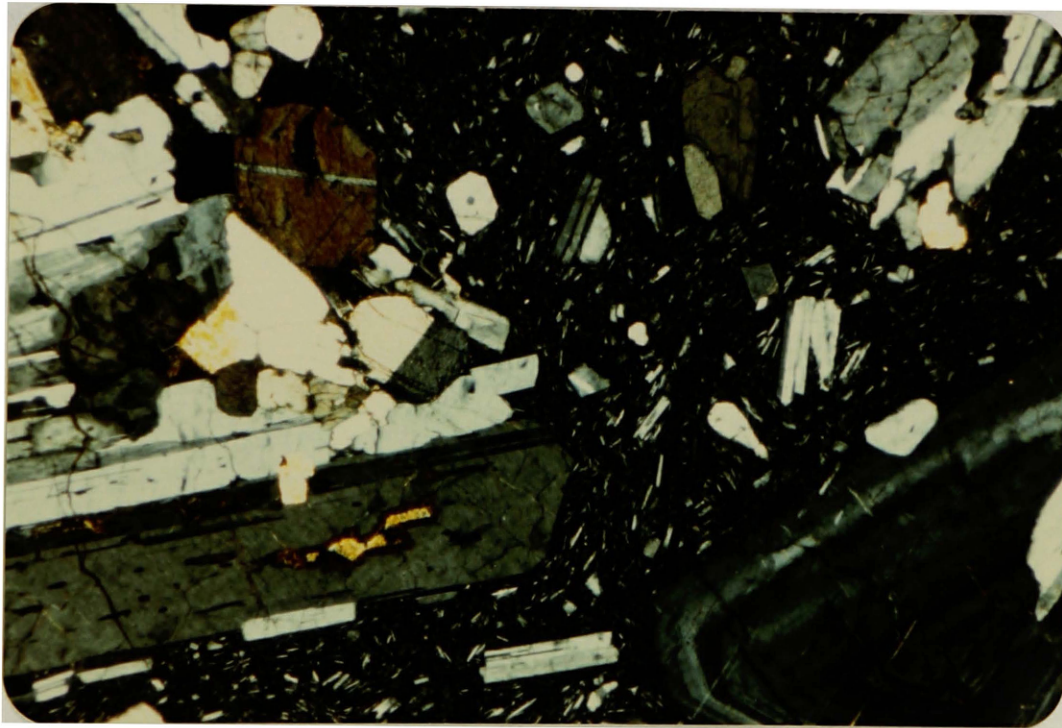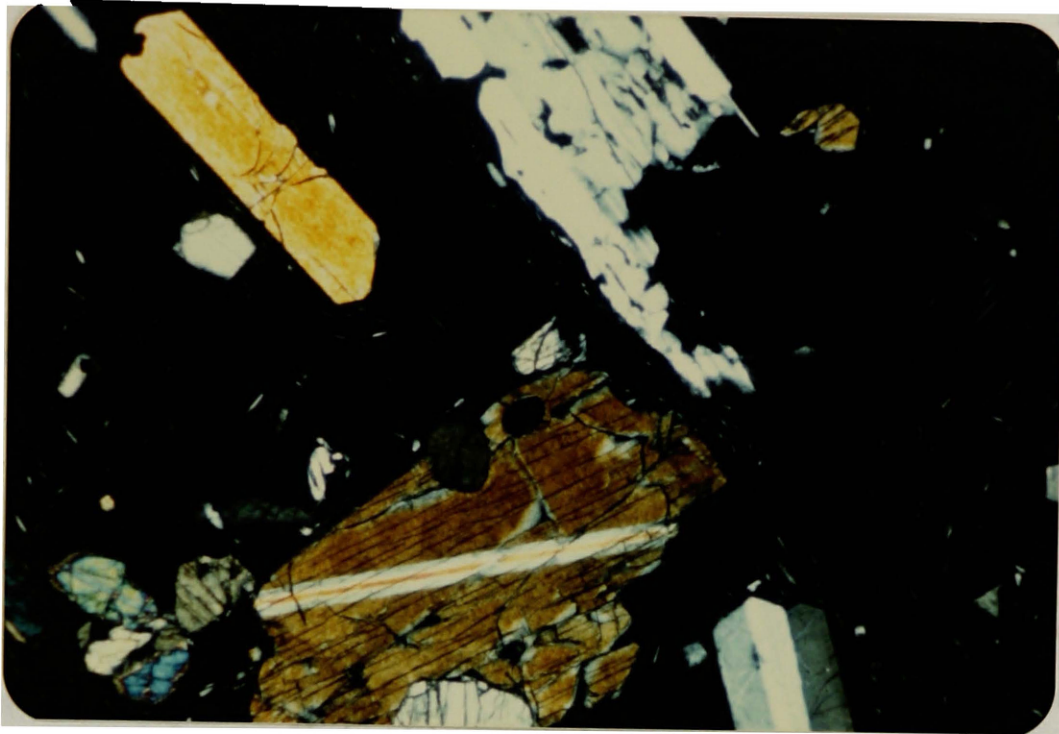
Figure 7 : Photomicrographs of two-pyroxene andesites showing
porphyritic (above) and glomeroporphyritic textures.
Note the two periods of plagioclase crystallization;
early corroded (upper) or resorbed (lower) and later
pristine and well twinned crystals. Field of view
about 1 cm across. Crossed polars.

locally filled with secondary minerals which include calcite, clay, chlorite, epidote, quartz and magnetite.

The lower pyroxene andesite sequence is capped by a series of glassy, maroon to black, porphyritic two-pyroxene andesites and minor hornblende-biotite andesite best exposed in the northwest portion of the map area where they underlie younger welded rhyolite tuff (Trt). Exposures are commonly characterized by large hackly, conchoidally fractured boulders measuring up to two meters in diameter. Upper two-pyroxene andesites are almost identical to underlying andesites in phenocryst content, mineralogy and texture but differ markedly by the abundance of intersertal glass in the groundmass. They also are characterized by a higher silica and alkali content than underlying two-pyroxene andesites (Table 1).

Dacite (Td)

Scattered float of light green, coarsely porphyritic biotite hornblende dacite is strewn over an area of about 40 square meters in the northwest corner of section 4, T21S, R32E. This unit consists of four to five percent resorbed and commonly zoned plagioclase phenocrysts up to 0.5 centimeter and three to five percent combined hornblende and biotite microphenocrysts all set in a fine-grained intergrowth of quartz, feldspar and clay (Figure 8). Quartz locally forms crystals up to 0.5 millimeter in diameter. Biotite is commonly rimmed with opaque oxides and locally replaces hornblende. The stratigraphic relationship between this unit and surrounding andesitic flows is not known because
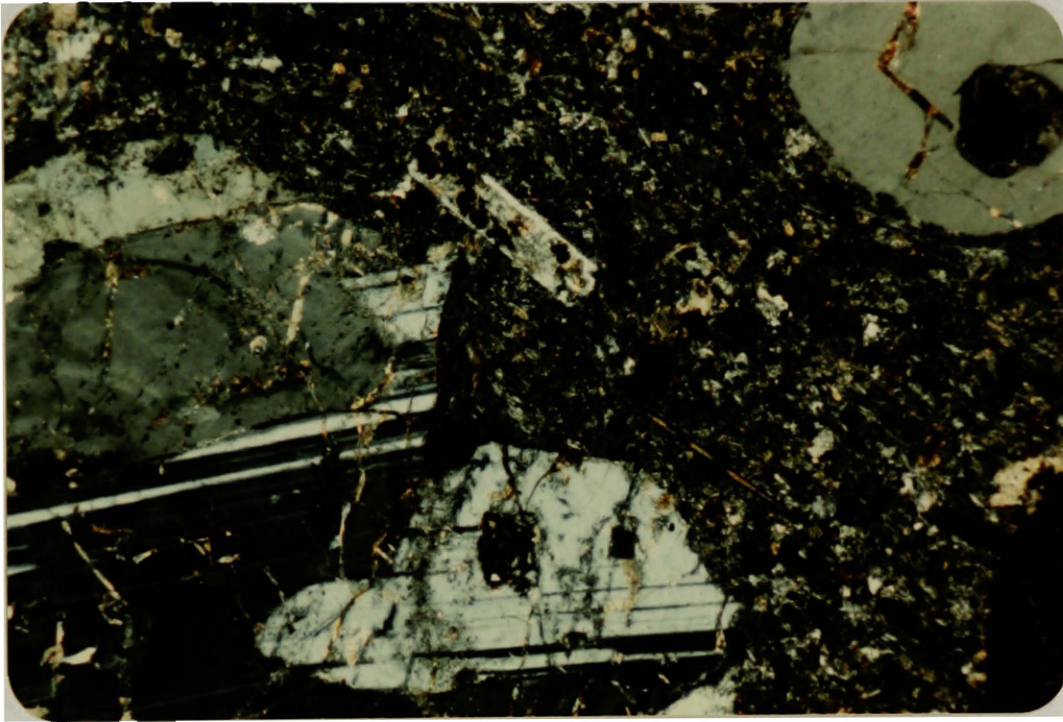
Figure 8 :   Photomicrograph of porphyritic dacite showing
             coarse, rounded, and resorbed quartz and plagio-
             clase phenocrysts in a fine-grained clay, chlorite,
             biotite-altered groundmass. Horizontal field of
             view approximately 1 cm. Crossed polars.

geologic mapping was not continued to the north.

Basalts (Tb)

Two isolated and mineralogically distinct basalt units cap pyroxene andesite along the eastern margin of the map area (Figure 9). The southern basaltic unit, exposed on the ridge east of Soldier Creek (E1/4, Sec. 16, T21S, R32E), is a dense, black, aphyric unit which weathers to rounded knobby ledges measuring up to 20 meters thick. In thin section this unit is composed of a dense ophitic growth of plagioclase and augite with minor intergranular olivine, opaque oxides and glass.

Basalt along the northeast margin of the map area is a black, sparsely porphyritic and locally vesicular unit which shows well developed thin platey jointing. Weathered surfaces are coated by a thick hematite-stained rind. This basalt consists of five percent subhedral plagioclase phenocrysts up to 3.5 millimeters in length set in a randomly oriented intergrowth of plagioclase microlites, augite, olivine, opaque and hematite-stained oxides, and minor glass.

Rhyolite Intrusions (Tr)

Porphyritic rhyolite dikes and small plugs intrude andesitic volcanics throughout the map area. The most prominent is a dike measuring 15 to 25 meters thick, and extending over a distance of 1.5 kilometers along a N60E trend. This and other rhyolite intrusions
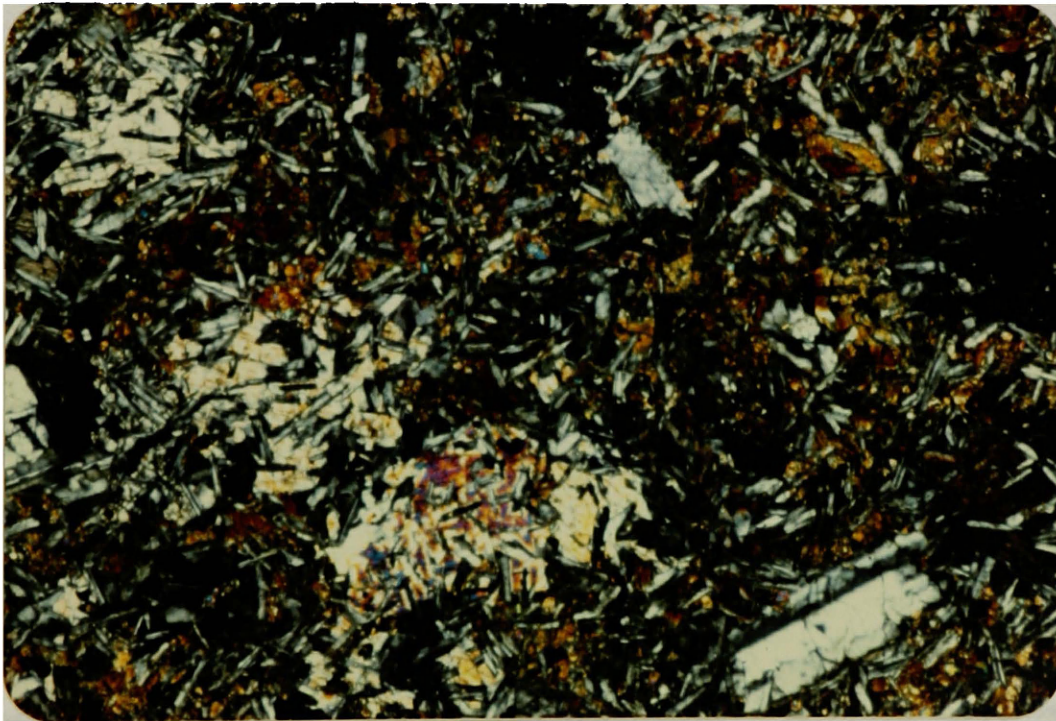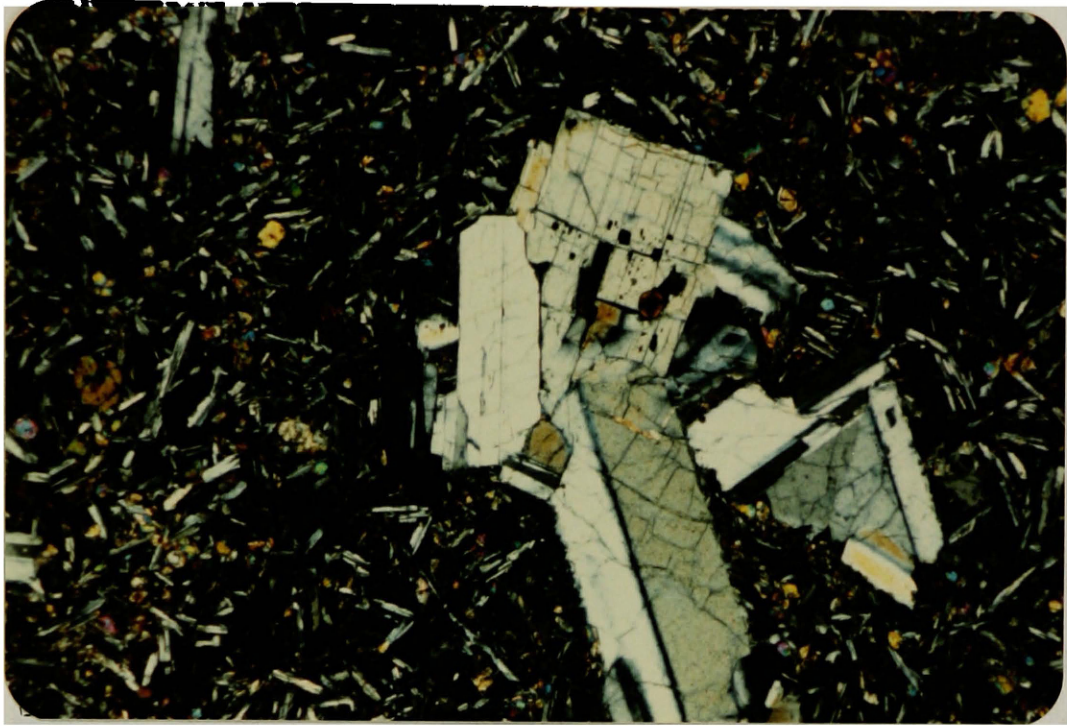
Figure 9 : Photomicrographs of different basalt units. Upper photo shows plagioclase glomerocryst with intergranular olivine, plagioclase and glass. Lower photo exhibits dense ophitic intergrowth of augite and plagioclase microlites. Horizontal field of view approximately 1 cm. Crossed polars.

contain 10 to 15 percent combined quartz and sanidine phenocrysts in about equal proportions set in a very fine-grained, white, felty, sericitized and locally silicified groundmass (figure 10). Phenocrysts, ranging in size from 0.5 to 1.5 millimeters in diameter, are subhedral to euhedral and locally rounded and resorbed. Some rhyolites contain minor pyrite cubes or casts and local manganese oxide staining.

Quartz-Porphyry Granitic Intrusions (Tqp)

Three coarsely porphyritic to equigranular granitic bodies intrude the andesite sequence in the vicinity of Gold Gulch (Figure 11). All exposures are very small, measuring less than ten meters in diameter. Two granitic bodies located between the north and south breccia zones are characterized by 25 to 35 percent rounded and resorbed quartz phenocrysts up to one centimeter in diameter set in a fine- to medium-grained (≤ 3 mm) feldspar and mafic (3%) groundmass. Feldspars are moderately to strongly altered to clay and sericite; mafics are chloritized. Intrusions locally contain abundant (5%) bvoid myrolitic cavities which are commonly jacketed by clay coronas and locally quartz filled.

The third granitic body, located southeast of "Idol City Mines" along Wickerbill Gulch, locally exhibits a coarse-grained hypidiomorphic granular texture in addition to porphyritic textures. Equigranular varieties consist of strongly resorbed and fractured interlocking quartz and sericitized feldspars up to one centimeter in diameter. Feldspars locally exhibit relict twinning, zoning and perthitic (?) textures.
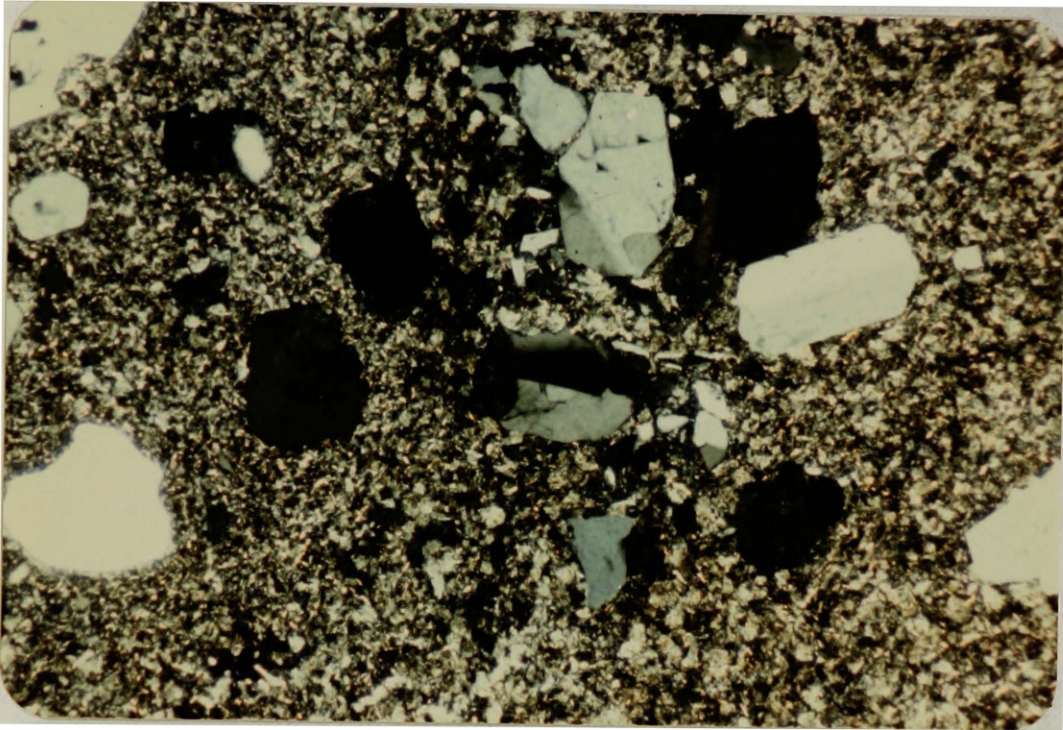
Figure 10:   Photomicrograph of porphyritic rhyolite intrusion
             showing resorbed quartz (left) and fresher, twinned
             sanidine (right) phenocrysts in a felty quartz,
             sericite groundmass. Horizontal field of view
             approximately 1 cm.
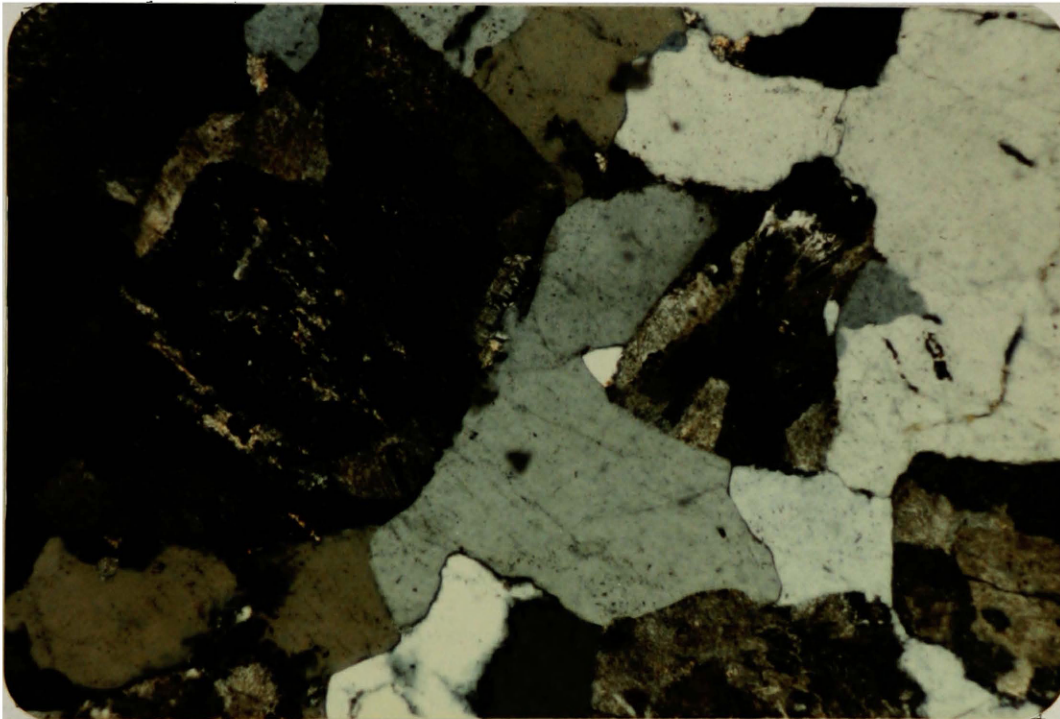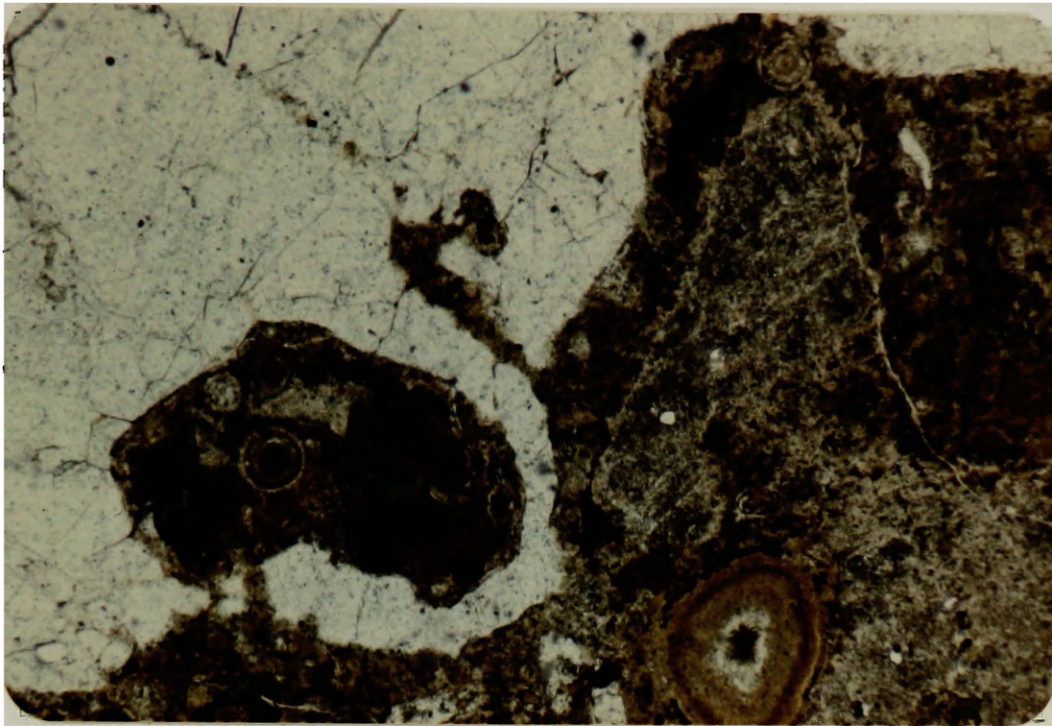
Figure 11:   Photomicrographs of different textural varieties
of granitic intrusions. Quartz porphyry variety
(above) comprised of coarse resorbed quartz pheno-
crysts in finer groundmass containing myrolitic
cavities. Hypdiomorphic granular texture shown
in lower photo. Horizontal field of view approxi-
mately 1 cm. Upper photo plain light; lower
polarized.

Quartz locally contains minor secondary tourmaline.

Rhyolite Welded Tuff (Trt)

Unconformably overlying andesitic flows on the west and south edge
of the property is a moderate to densely welded rhyolite ash-flow sheet.
This greenish-grey, crystal-rich rhyolite tuff forms a prominent
resistant cap up to ten meters thick over younger intermediate flows.
Outcrops are characterized by well developed compaction foliation,
widely spaced joint surfaces, locally abundant lithophysal cavities, and
irregular hackly weathered surfaces. Rhyolite tuff post-dates the
mineralizing episode and thus usually marks the extent of geologic
mapping.

This unit consists of ten to 15 percent combined quartz and
sanidine phenocrysts up to 2.5 millimeters in length and minor (0.5%)
sodic pyroxene set in a vitroclastic matrix. Locally abundant pumice
lapilli are moderately to strongly flattened (Figure 12). Feldspar and
quartz are commonly shattered, rounded, and resorbed.

Latite Lapilli Tuff (Tlt)

Capping basaltic units on the east edge of the map area are
discontinuous exposures of pink to pinkish-grey poorly welded latite
lapilli tuff. This unit rarely crops out, but rather forms broad areas
of platey float. It is composed of 15 to 30 percent angular to rounded
felsic pumice lapilli up to five centimeters in diameter. Pumice
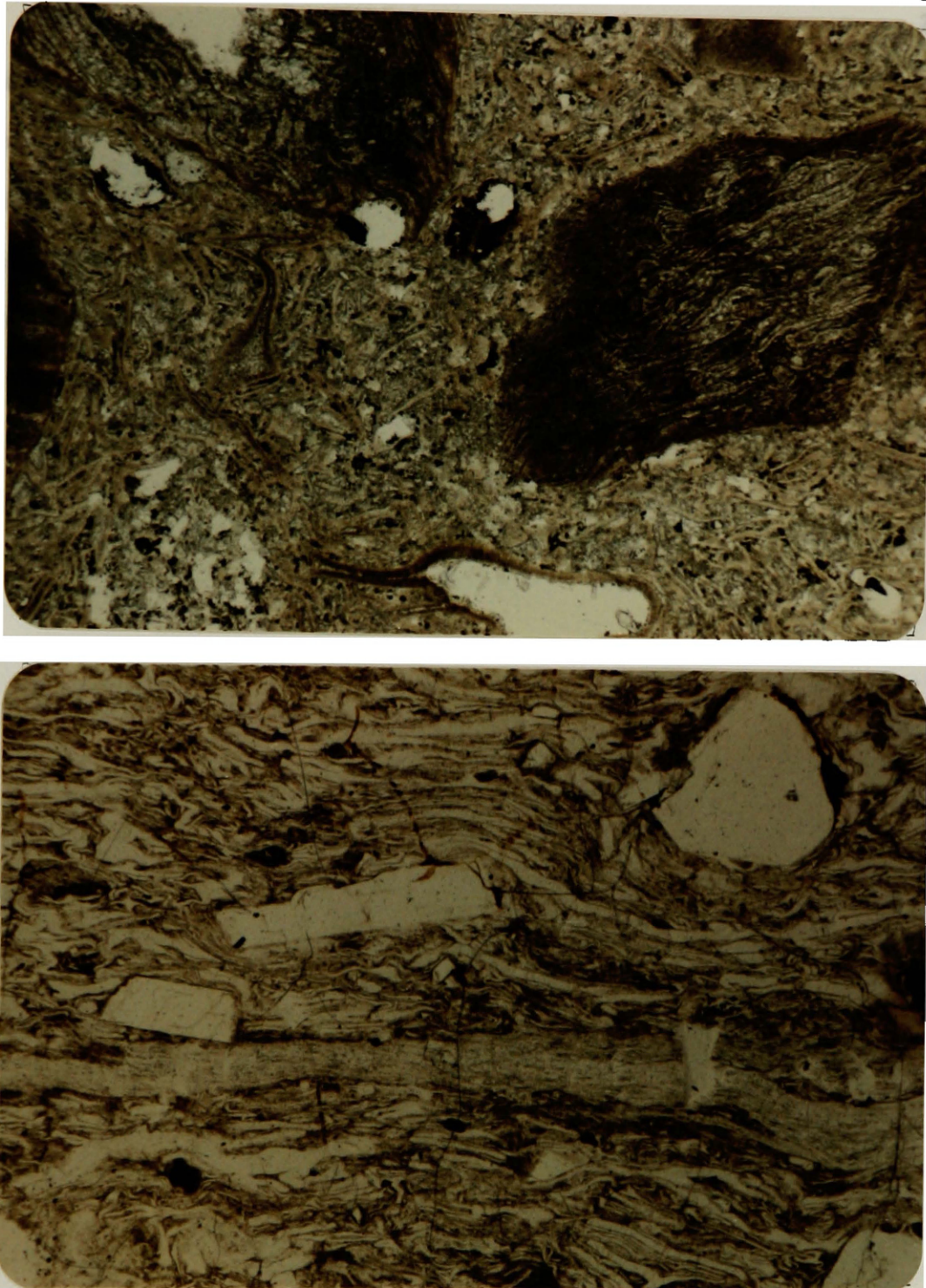
Figure 12: Photomicrographs of different ash-flow tuff units.
Note the differences in degree of flattening of
pumice fragments and glass shards in the poorly
welded latite lapilli tuff (above) and densely welded
rhyolite tuff (below). Horizontal field of view ap-
proximately 1 cm. Plain light.

fragments rarely show flattening and are set in a punky, devitrified, vitroclastic matrix containing minor (3% combined) broken subhedral to anhedral plagioclase and K-feldspar crystals up to 1.5 millimeters (Figure 12). Lapilli fragments are locally differentially weathered giving the rock a honeycomb-like appearance.

Age and Correlation of Rock Units

Intrusive and extrusive activity in the Idol City area occurred over a period of at least 11 million years. Potassium-argon age dates of 19 $\pm$0.8 million years on a rhyolite dike (Tr) and another of 21 $\pm$0.9 million years on sericite alteration in the Idol City area (Appendix B) places a minimum age of about 20 million years on intermediate lavas which form the core of the study area. These lavas are part of a regionally extensive basalt and andesite unit which yielded dates ranging from 12 to 21 million years (Walker, 1979; Greene and others, 1972; Christiansen and Lipman, 1972). Stratigraphic relationships within this unit, which include the Strawberry volcanics, Columbia River Group, Owyhee basalt, and Steens Mountains volcanics are poorly understood. However, intermediate-composition volcanics at Idol City most closely correlate with calc-alkaline lavas of the Strawberry volcanic field to the north.

Welded rhyolite tuff (Trt) which unconformably overlies andesites on the west edge of the property is nine to ten million years old in adjacent areas, and correlates with the moderate to strongly welded basal section of the Devine Canyon tuff (Greene, 1973). Poorly welded

lapilli tuff on the east edge of the map area shares many characteristics with the Prater Creek tuff, a devitrified crystal-poor tuff which has been dated at 8.⁴ million years (Walker, 1979). Both tuffs were erupted from calderas nested in Harney Basin to the south (Figure 4).

Structures

Faults

Numerous high-angle faults and shears cut the volcanic sequence; however, very few can be traced for significant distances due to poor exposure. Major faults are generally inferred on the basis of linear alteration and/or geomorphic trends, and geophysical data. Structural trends are also substantiated by geochemical data; zones of metal enrichment commonly coincide with structural trends (Figures 20 and 22).

In general, faults and shears can be classified into three groups. Each group shares similarities in character, distribution, continuity, and possibly timing. The dominant structural trend is a series of narrow, continuous, north-trending, high-angle faults which are rarely mineralized and commonly offset mineralized structures and stratigraphy. The largest fault in this group extends for over two kilometers through the western part of the map area, and juxtaposes hydrothermally altered hornblende andesites in the vicinity of the north breccia, with fresh pyroxene andesites to the west (Plate 2). Similar faults offset a rhyolite dike and a vein in the north part of the map area. These

north-tending structures probably represent the youngest episode of faulting.

The structural pattern in mineralized areas is dominated by what appears to be a conjugate set of northeast- and northwest-trending fault systems. These fault systems trend N40-70W and N40-60E. The northwest trend is particularly evident on the east flank of Gold Gulch, where a series of discontinuous shear zones converge with the north breccia body. Individual shears measure up to five meters in width, show minor offset, and are commonly mineralized.

In contrast, the northeast trend is defined by the dominant structural grain (southwest-northeast elongation) of both breccia bodies. Although faults could not be identified in either breccia zone from surface geology, gouge was encountered in several drill holes. Additionally, a major rhyolite dike located in the northern part of the map area parallels this northeast trend.

Breccia Zones

Alteration and mineralization are centered about two large zones of brecciation and fracturing believed to have formed in part by explosive hydrothermal activity (see page 65). The largest, the south breccia, forms a prominent hill just south of Gold Gulch. This zone is about 500 meters in length and 200 meters in width. The north breccia, located near the head of Gold Gulch, measures about 400 meters by 200 meters. Both zones are roughly tabular showing a southwest-northeast elongation.

Breccia zones are a composite of several breccia types. Characteristics of the different types are given below, and spatial relationships are illustrated in Figure 13.

Tourmaline breccias - rounded to angular clasts, clast or matrix supported, mixed clasts, rotation or transport of clasts, tourmalinized matrix, irregular distribution.

Stockwork breccias - angular clasts, clast supported, little to no rotation of clasts, several episodes of veining, widely distributed.

Rubble breccias - angular to rounded clasts in an unconsolidated rock flour matrix, clasts commonly of a single lithology and alteration type, isolated distribution, offset stockwork zones.

Both breccia zones are characterized by an abundance of introduced tourmaline. The distribution of tourmaline breccia varies considerably between the "north" and "south" breccia zones, as indicated in Plates 3 and 4. The north zone is almost exclusively comprised of tourmaline breccia, whereas in the south zone tourmaline breccias occur as a network of isolated pipes, dikes or pods.

Tourmaline breccias exhibit a wide variety of textures (Figures 14 and 15). All degrees of angularity, size, sorting, and cementation of fragments occur. Fragments generally range from sand to fist size; however, boulder size fragments were seen. Some breccias are composed
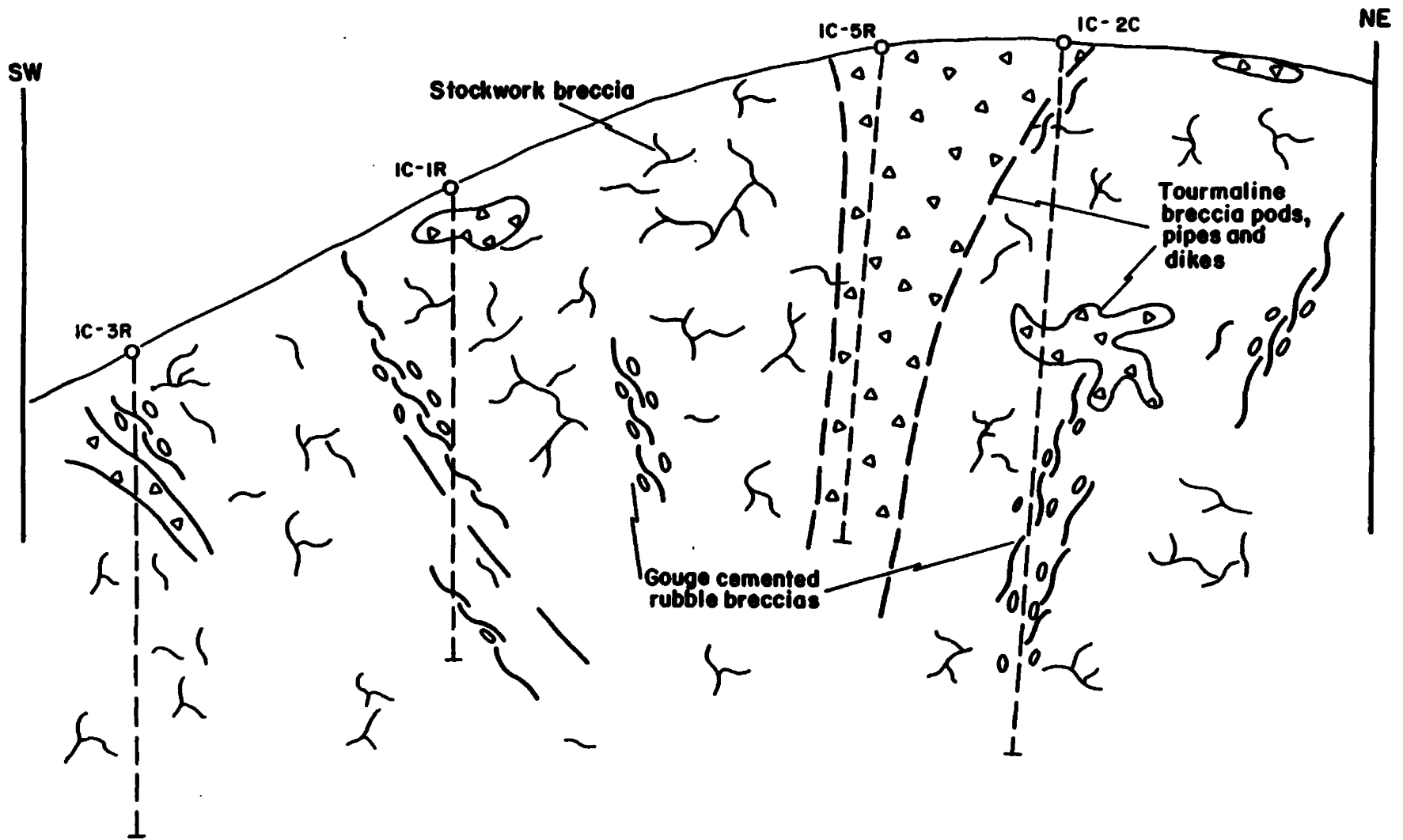
Figure 13: Distribution of different breccia types in south breccia zone. Isolated shears and irregular shaped tourmaline breccia bodies are located within a broad area of stockwork breccia. Drill hole locations are given for reference. Detailed drill logs are given on Plate .
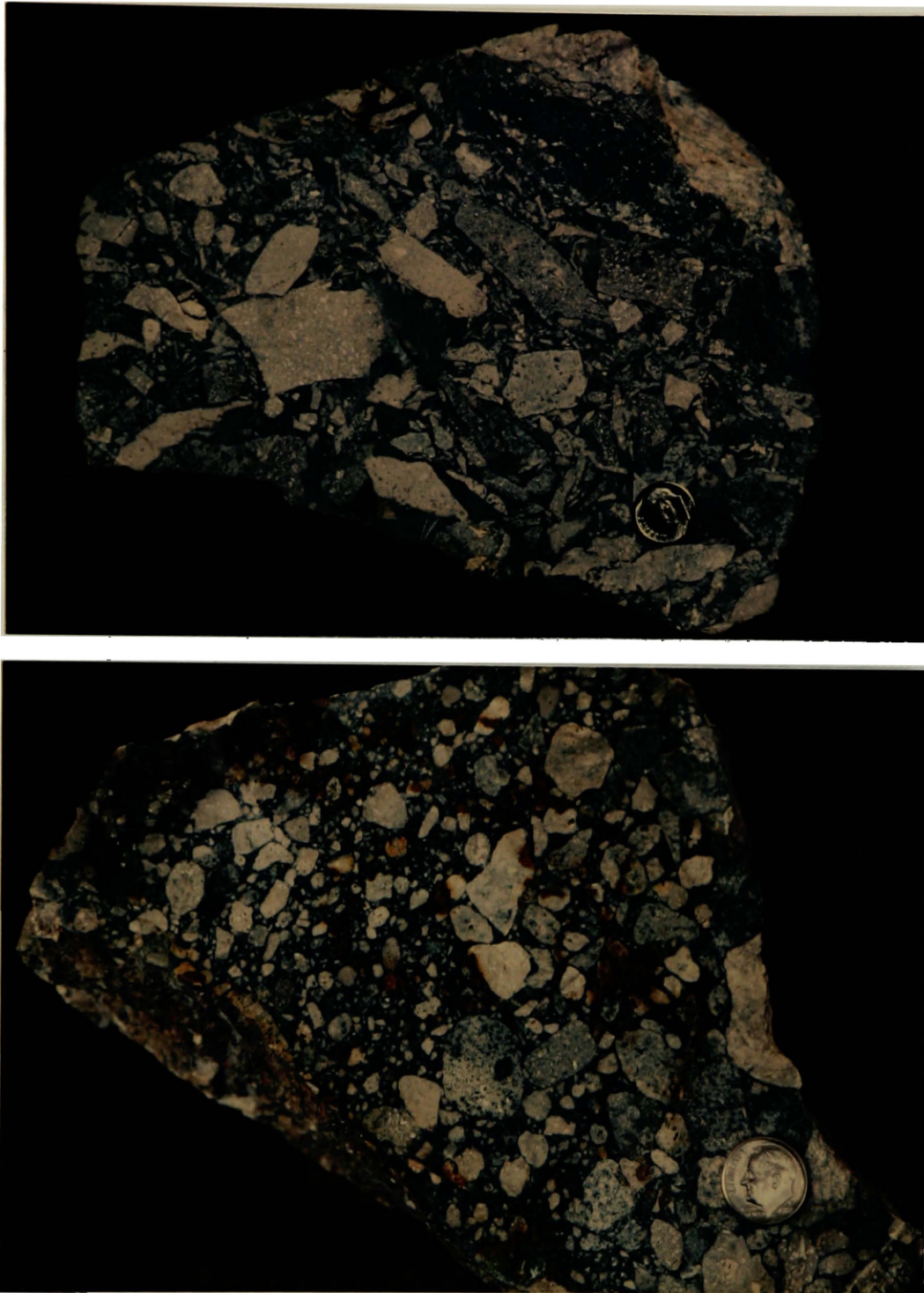
Figure 14: Photographs of different textural varieties of tourmaline breccias. Upper sample comprised almost exclusively of angular clasts supported in a finer quartz-tourmaline (blue) matrix. Note preferred orientation of tabular clasts. Lower sample is both clast and matrix supported, exhibits a distinct grading in clast size and angularity, and shows mixing of clasts of different lithologies and alteration types.

strictly of angular clasts with little to no matrix. Others are composed almost exclusively of rounded fragments supported in a fine-grained silicified and tourmalinized rock flour matrix.

Tourmaline breccias are commonly heterolithologic, composed of fragments showing a variety of textures and alteration types. Fragments are commonly remnants of earlier stages of fracturing and stockwork veining. The primary mineralogy of fragments is usually destroyed by alteration; however, most have textures resembling andesitic flows.

Fragment transport can be recognized in many samples by the strong preferred orientation of fragments. Smaller tabular fragments commonly exhibit a pilotaxitic-like texture about larger fragments (Figure 15). Additionally, some samples exhibit a size gradation of fragments (Figure 14).

Tourmaline breccia bodies are enclosed in broad zones of fracturing and stockwork veining. These stockwork breccias contain angular, irregular-shaped clasts showing little to no rotation and generally exhibit strong degrees of quartz-sericite ± minor tourmaline alteration (Figure 16). These zones represent the most important hosts for base- and precious-metal mineralization.

Stockwork zones are commonly reduced to gouge-cemented rubble breccias upon shearing. The best example of this is preserved in the lower part of the hole IC-83-2C, where rubble breccias extend continuously between 317 ft - 440 ft (Plate 3).
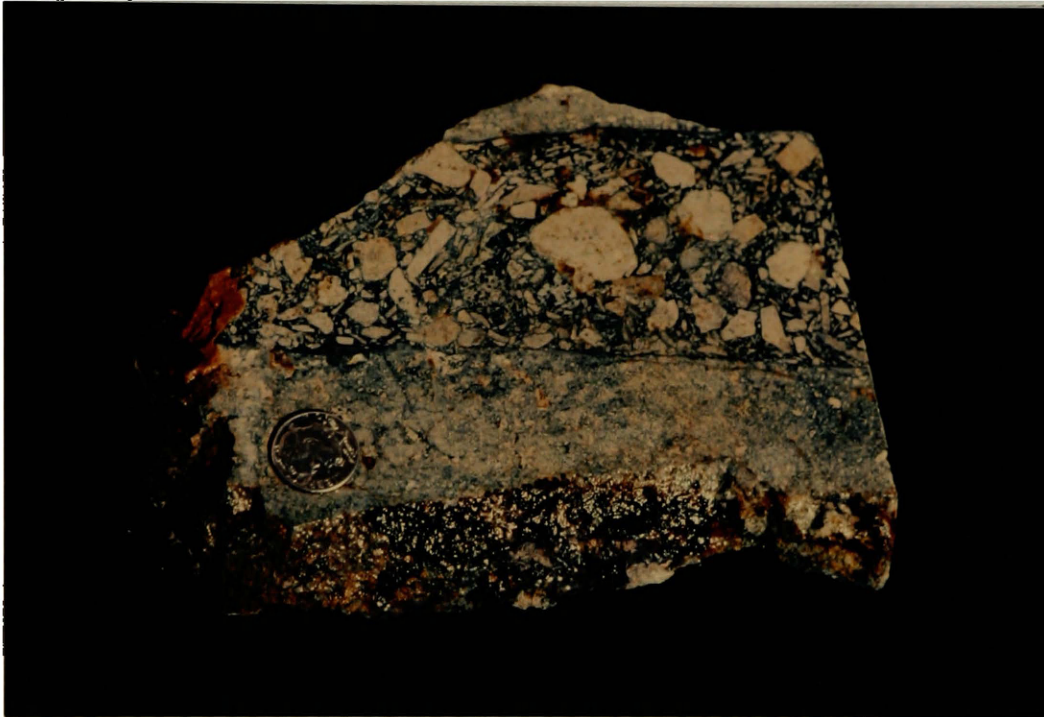
Figure 15: Photograph of a late stage tourmaline breccia dikelet showing a wide variability in fragment size and angularity. Small tabular fragments exhibit a pilotaxitic-like texture about larger fragments.

Figure 16: Photograph of stockwork breccias from core hole
IC-1C. Samples comprised of angular fragments
showing little to no rotation healed by quartz-
sulfide microveinlets.

Rubble breccias are characterized by angular to rounded silicified fragments measuring up to 15 centimeters in diameter set in a sandy to pebbly unconsolidated clay-rich matrix (Figure 17). Fragments usually show no preferred orientation and are generally of a single lithology and alteration type. Fragments are commonly fractured and stockwork veined prior to brecciation. Brecciation is locally followed by disseminated or fracture controlled mineralization which is generally confined to gougy matrix material.

Folds

Mineralized rocks at Idol City lie along the axis of a regional south plunging anticline (Figure 4). Folding is recognized in the study area by a progressive younging of rock units east, west, and south of the Gold Gulch region. Moderately to steeply dipping compaction folliations measured in ash-flow sheets (Plate 1) indicate folding post-dates the mineralizing event.

Hydrothermal Alteration

The degree of hydrothermal alteration varies widely throughout the Idol City area. The most intense alteration is associated with zones of structural complexity. Alteration is confined to intermediate lavas and felsic intrusions. Overlying ash-flow sheets post-date the alteration episode. The distribution of alteration types in mineralized areas was mapped at a scale of 1"=200´ (Plate 2). Alteration in drill holes is
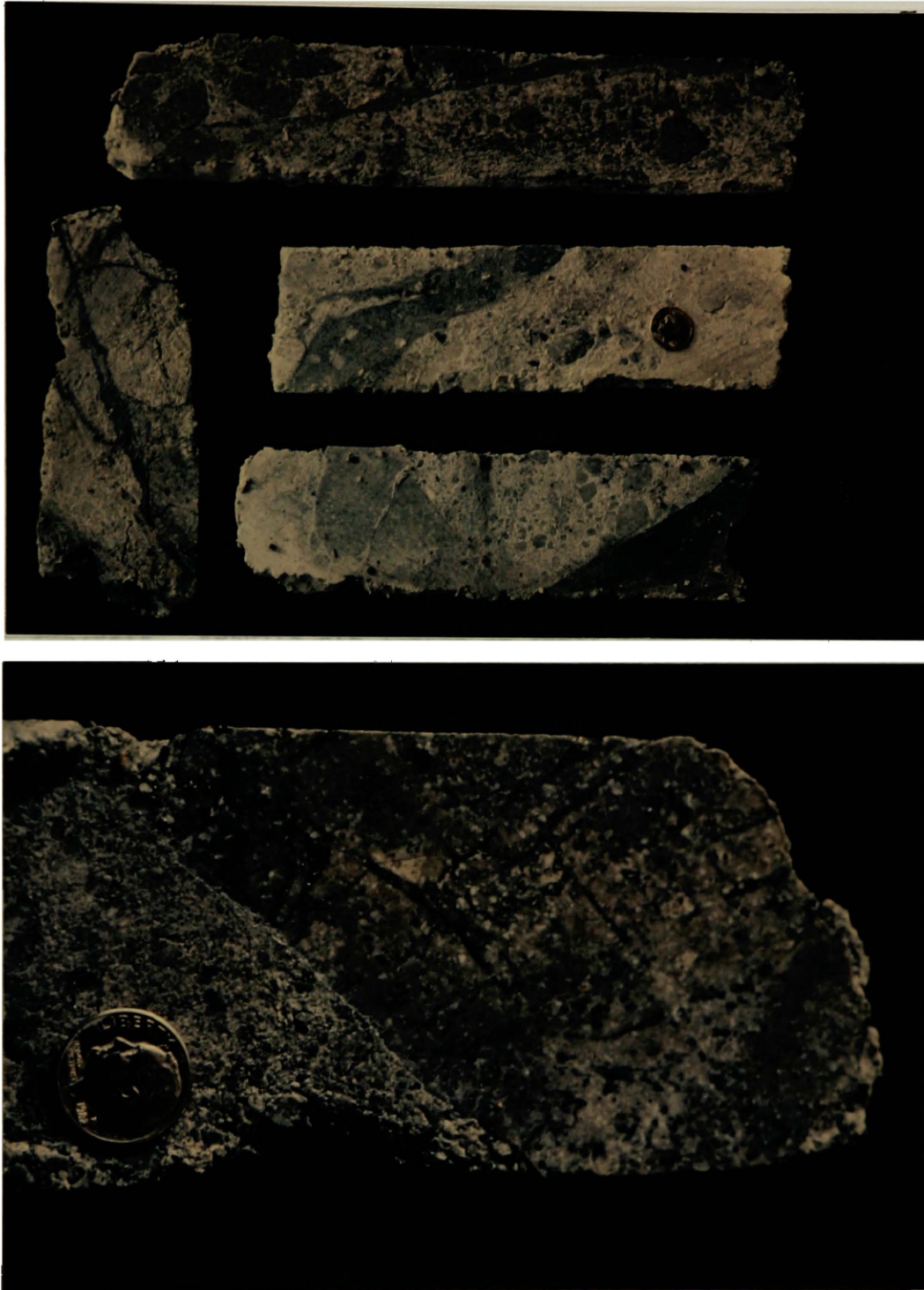
Figure 17. Photographs of rubble breccias showing rounded to
angular silicic fragments in a sandy to pebbly
clay-rich matrix. Fragments are commonly remnants
of earlier periods of stockwork veining.

displayed in Plates 3 and 4.

Four types of alteration were distinguished on the basis of color, texture, and kinds and intensity of secondary minerals present. Secondary minerals were identified in several samples by petrographic and X-ray diffraction methods.

Clay mineral determinations on 20 samples were made on a Phillips X-ray diffractometer according to methods described by Thompson (personal comm., 1983). The less than two micron clay fraction was separated by gravity and placed on a glass slide. Samples were subjected to a series of temperature and chemical treatments prior to X-ray analysis. Results are listed in Table 2 and sample locations are shown on Plate 2.

Tourmalinitic

Breccia zones are characterized by introduced fine-grained tourmaline which gives rocks a distinctive blue color. Tourmaline is dravite, a high-magnesium variety. It occurs as disseminations or dense intergrowths of radiating acicular crystals measuring up to 0.1 millimeter, and is usually associated with strong silicification and sericitization.

Variations in the intensity and distribution of tourmaline correlate well with changes in the style of brecciation. Tourmaline occurs in minor amounts (generally <2%) associated with stockwork zones; whereas, isolated breccia pipes and dikes contain up to 25% introduced tourmaline.

The transition between strongly tourmalinized rocks and other alteration assemblages appears to be fairly abrupt based on surface exposures and drill data. An abrupt transition is evidenced at a small scale in at least one sample where a well defined tourmalinized breccia dikelet cuts an earlier quartz-sericite-minor tourmaline assemblage (Figure 15).

Sericitic

Sericitic alteration is commonly associated with shearing and intense fracturing within and adjacent to breccia zones and related to felsic intrusions. Although an abundance of white mica characterizes this zone, rocks usually contain important amounts of kaolinite, and locally smectite (Table 2). In addition, a 9A mineral, probably pyrophylite, was identified in one sample.

Sericitized volcanic rocks are distinguished by the complete destruction of phenocrysts and groundmass minerals by mica and clays giving rocks a white, punky appearance. Sericitic alteration of rhyolite intrusions is confined to the groundmass; sanidine and quartz phenocrysts are generally fresh.

Quartz veining, silicification, and introduced pyrite are also important and commonly diagnostic of sericitized rocks. Groundmass minerals are generally converted to a patchy intergrowth of fine-grained quartz and clays and commonly contain two to three percent pyrite as disseminations or filling veinlets.

TABLE 2: Clay Mineralogic Determinations

Geologic Setting	Sample	Sample Treatments	Sericite	CI*	Kaolinite	Smectite	Other
	5258	G, H	+	6.6	+	-	
	1567	A, G, H	+	11.0	+	+	
North	5321	A, G	+	7.1	+	+	
Breccia	5304	A, G, H	+	3.7	+	-	
and	5302	A, G, H	+	4.4	+	+	
Associated	1563	A, G, H	+	4.2	-		Pyropholite?
Rocks	6995	A, G, H	+	7.6	-		
	5313	A, G, H	+	6.1.	+	-	
	5255	G	+	11.4	+	+	
	1593	A, G, H	+	20.5	+	-	
	10960	A, G, H	+	12.0	+	-	
Remote	5324	G				-	Chlorite
Propyli-	802	A, G	-		+	+	Chlorite
tized Andesites	6969	A, G, H	+	11.9	+		Chlorite
Felsic	IC-5	A, G, H	+	7	+	-	
Intrusive	6846	A, G	-	23	-	+	
Rocks	6889	G	+	6.9		-	Chlorite
	5264	G	+	7.4	+	-	
South	5267	G	+	2		-	
Breccia Zone	5270	A, G, H	+	5.1	+	+	

Sample Treatments: Air Dried (A), Glycol Solvated (G), and Heated.

Concentrations: Major (+) and Minor (-).

CI* (Crystallinity Index): Lower values reflect higher degree crystallinigy, calculated by method of Kubler (1963).

All analyses conducted on the <2 micron size fraction. Sample locations given on Plate 2.

Sericitic alteration is generally gradational with surrounding argillic and propylitic assemblages. Furthermore, the intensity of sericitization varies progressively within individual altered zones. X-ray diffraction analyses of several samples across the broad sericitized zone along the east edge of the north breccia revealed a transition in the crystallinity of micas from the margins inward (Table 2). Mica 10A peaks become progressively sharper toward the tourmalinized zone, indicating a higher degree of crystallinity.

Argillic

Weaker mica and clay alteration forms a broad halo around pervasively altered sericitic zones. The term argillic alteration is used to describe pinkish to orangish-tan rocks that show only partial destruction of phenocrysts and groundmass minerals by clays ± sericite, or areas of heavy cover which contain significant amounts of mixed propylitic and argillic/sericitic altered float.

Argillically altered rocks are characterized by the preservation of primary rock textures. Feldspars are usually pitted and only partially replaced by clays, and mafic minerals are commonly converted to pyrite or iron-oxides. These rocks commonly show weak to moderate degrees of silicification, especially in drill holes. Contacts between stronger and weaker alteration zones are usually gradational.

Propylitic

Propylitic alteration forms a broad halo about all stronger degrees of alteration and is gradational into fresher rocks. Propylitized rocks are distinguished by their medium to dark green color which is attributed to an abundance of introduced chlorite ± epidote. Feldspars commonly show partial to total replacement by calcite, clays, and locally chlorite. X-ray analyses indicate the presence locally of highly crystalline micas (Table 2). Mafic minerals are usually converted to chlorite, calcite, epidote and magnetite. Vesicles are usually lined by similar type alteration minerals, commonly concentrically zoned (Figure 18). Groundmass textures are typically enhanced giving rocks a pseudo-equigranular appearance.

Some propylitized rocks are extremely silicified and contain abundant introduced magnetite in addition to chlorite and epidote. Quartz-chlorite-epidote-magnetite-altered rocks are common within and adjacent to breccia bodies (Plates 3 and 4).

Mineralization

Gold Geochemistry of Soil and Rock Samples

Over 1,300 soil and 450 rock samples were collected over a four-year period to define source areas for placer deposits formed in the Gold Gulch drainage. The survey extends from just north of the Trout Creek-Gold Gulch confluence and extends southward for over three kilometers along the main alteration trend (Plate 1).
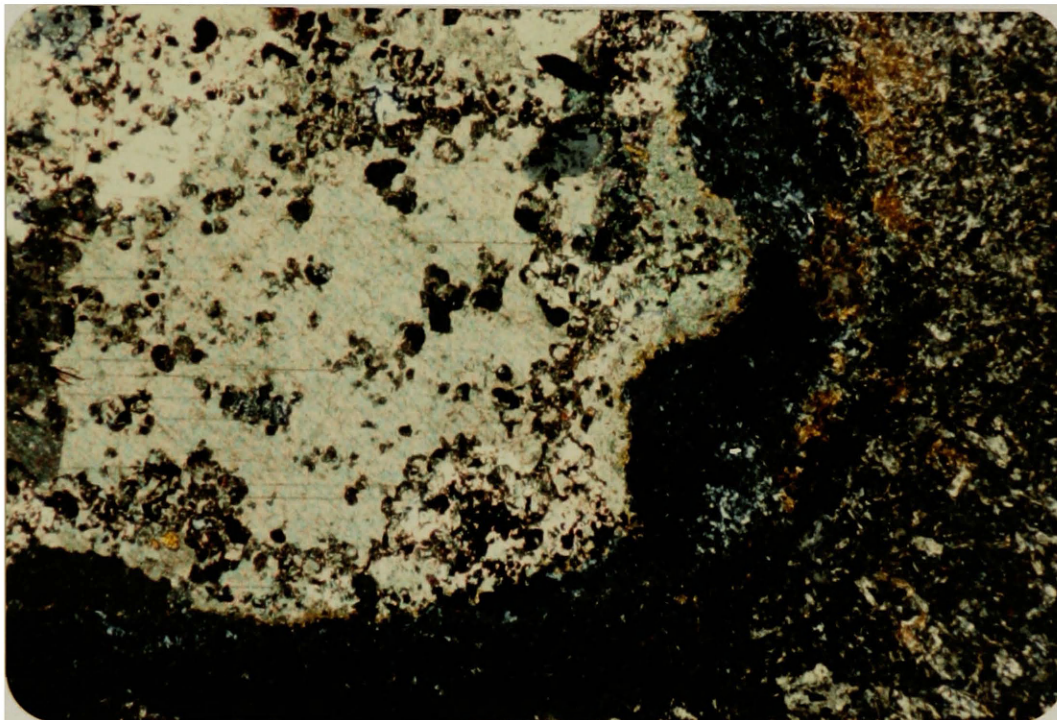
Figure 18: Photomicrograph of propylitized andesite. Note the zoning of alteration minerals within vesicle (upper left); calcite (pink and green), quartz (gray), epidote + chlorite (dark grey-blue), magnetite (black) from left to right. Horizontal field of view approximately 1 cm.

The survey identified broad areas of anomalously high gold centered around both breccia bodies, as well as several smaller scattered anomalies.

The south breccia shows a roughly symmetrical distribution of anomalously high gold which trends N40E (Figure 19). Soils contain up to 1.9 ppm gold; values greater than 100 ppb occur along a zone exceeding 400 meters in length and averaging 100 meters in width. The mineralized trend is open to the southwest, extending beneath alluvium.

The distribution of gold in soils in the north zone is much more irregular (Figure 20) and may be the result of thick overburden in this area. Contrary to soil results, rock samples show a strong N60E enrichment in gold over the tourmalinized zone which is deflected to the southeast on intersection with high-angle structures (Figure 21).

Geochemical results from four drill holes in the south breccia zone illustrate that subsurface gold grades are consistent over significant vertical and possibly lateral distances (Figure 24). Significant gold grades occur in three distinct zones over a vertical span of 150 meters. The largest zone, defined by anomalous to ore grade intercepts averaging about 60 meters thick in three holes and 20 meters thick in the upper part of IC-3R, is tabular and dips gently to the northeast along section. Although this zone spans a horizontal distance of over 300 meters and transcends various degrees of alteration and types of structural preparation, the magnitude and distribution of gold grades remains fairly consistent. This zone is unique because of the coincidence of gold with significant concentrations of base metals.
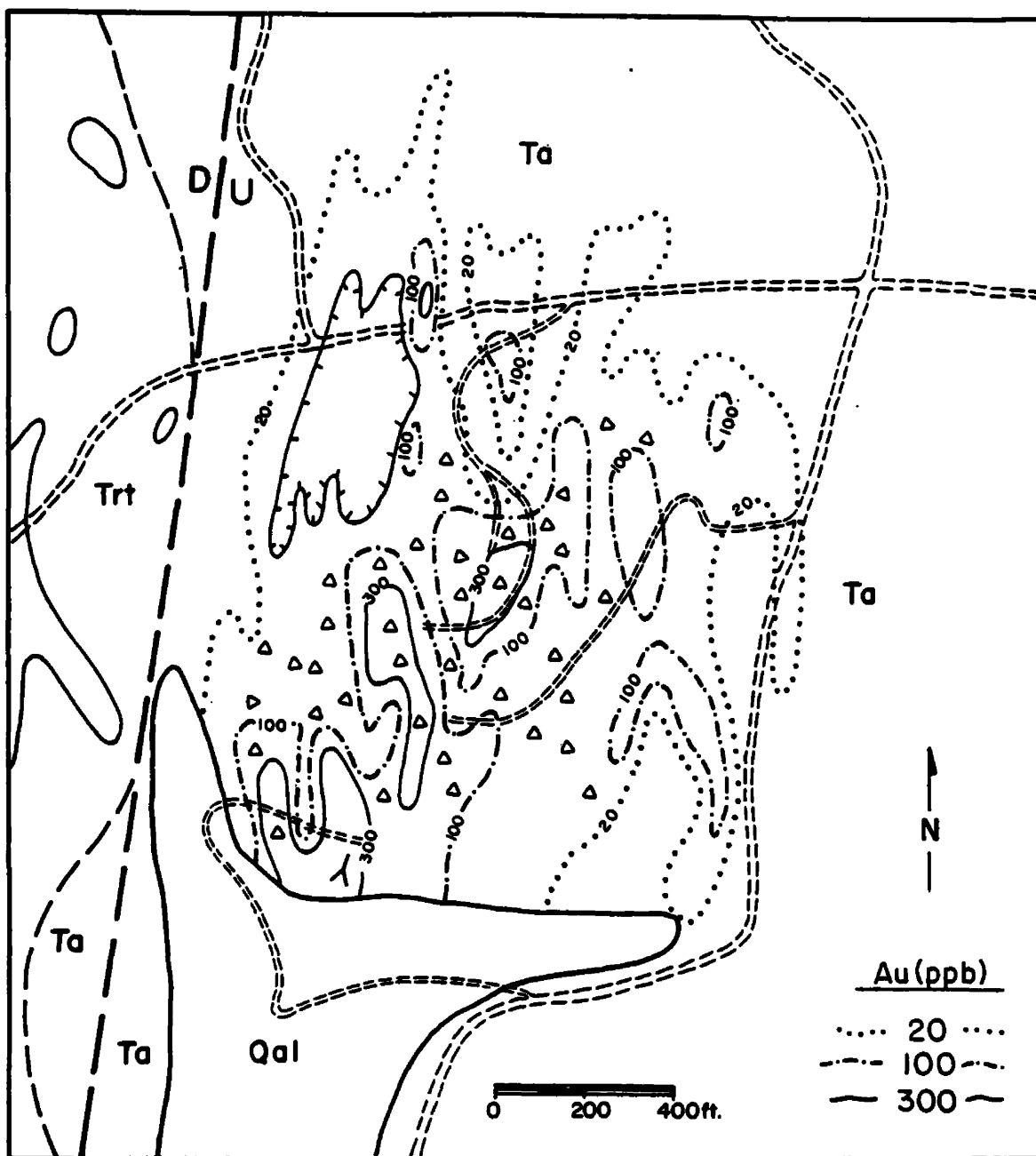
Figure 19: Soil sample gold geochemistry map of the south breccia zone. Contours are defined by about 250 samples collected at 50-foot intervals along N80°W-trending lines spaced about 200 feet apart. Geologic symbols as on Plate 1.
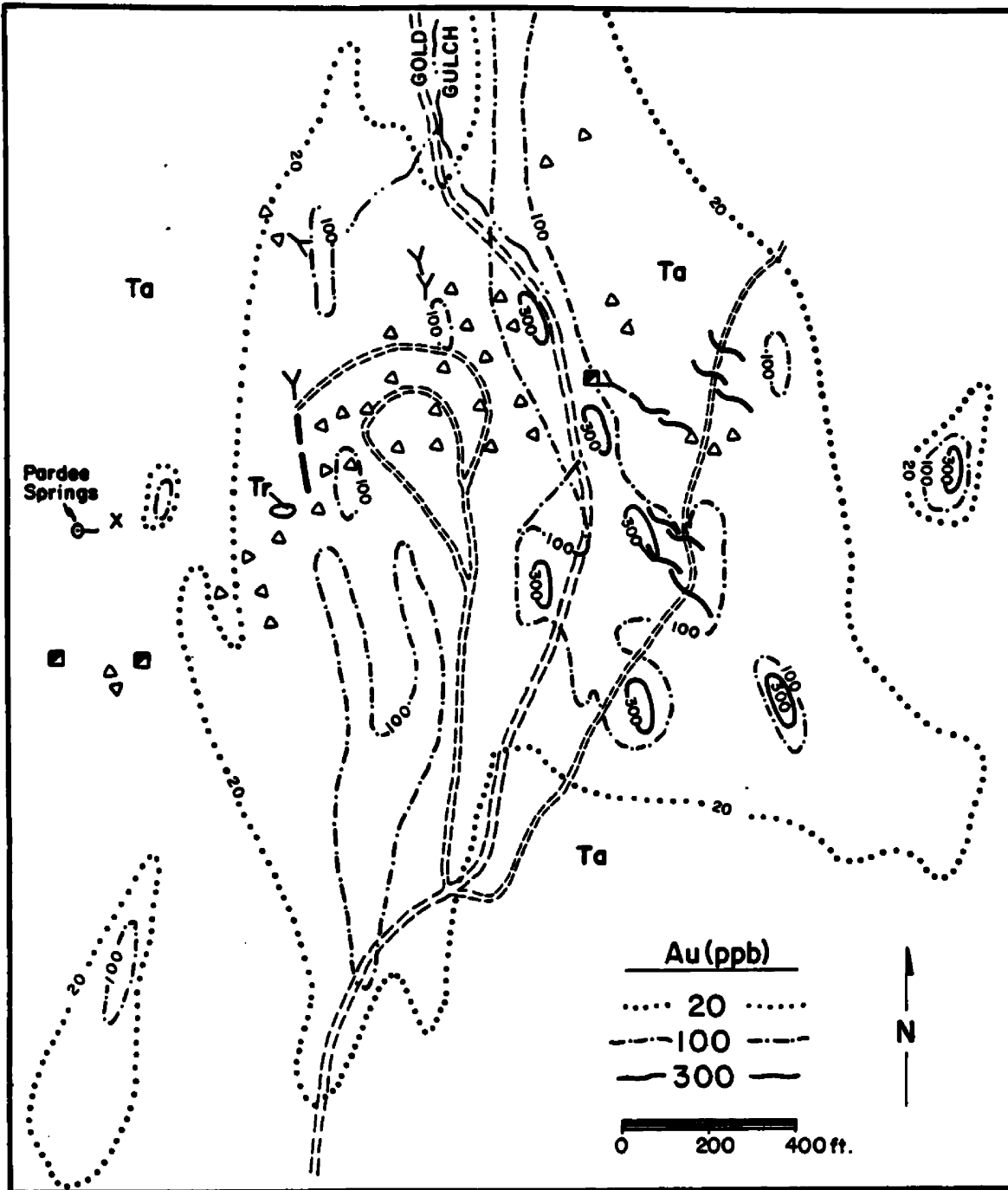
Figure 20: Soil sample geochemistry map of the north breccia zone.
Contours are defined by over 400 samples collected at
50- to 100-foot intervals along lines trending N80°W
at spacings of 200 or 400 feet. Geologic symbols as
on Plate 1.
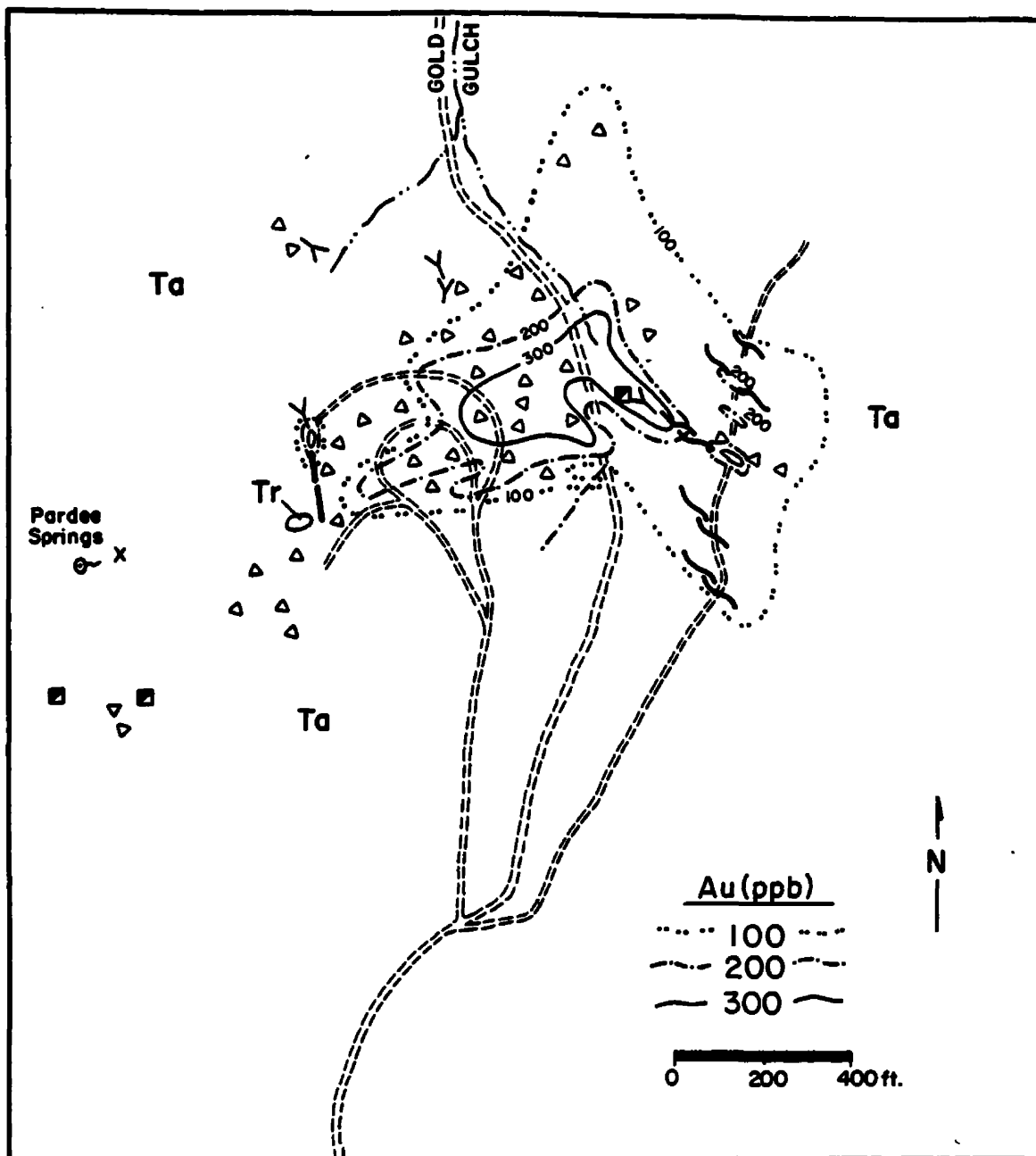
Figure 21:   Rock chip gold geochemistry map of north breccia zone.
Contours are based on over 150 rock chip and channel
samples.   Geologic symbols as on Plate 1.

Anomalously high lead, zinc, silver, and copper values are essentially confined to this gold-bearing horizon (Figure 25).

In contrast, two isolated, gold-rich zones measuring about 10 meters and 40 meters thick in the upper and lower parts of holes IC-5R and IC-3R, respectively, lack base metals. The lateral equivalent of the upper zone in IC-5R is evidenced by a weak gold anomaly in the upper part of core hole IC-2C to the north; it projects to the surface to the south. The lateral extent of the lowermost zone is uncertain because no other holes were drilled to the appropriate depths.

Despite high gold values from surface and subsurface samples, no visible gold has been identified on the property except in placers. Furthermore, panned concentrates from the highest-grade drill intercepts did not contain any free gold. This absence of free gold indicates that gold is in sulfide phases which are evenly dispersed (disseminated/stockwork) over broad areas. Young (1983) suggested gold may be in sulfosalts based on the direct relationship between gold and arsenic in panned concentrates from hole IC-1R.

Base-Metal and Iron Sulfides

Base-metal sulfides are widely distributed. They occur as disseminations and in veinlets within breccia and fracture zones, and locally as fissure deposits along high-angle shears. Sphalerite, the most abundant base-metal sulfide, is commonly associated with galena and chalcopyrite. Minor covellite, arsenopyrite and tetrahedrite were identified in polished sections from the upper part of hole IC-1C. Rare

fine-grained molybdenite flakes were seen in propylitized volcanic rocks in the upper part of hole IC-2R.

Although base-metals are common throughout several drill holes in both breccia zones, they do not presently constitute ore. Combined lead, zinc, and copper grades rarely exceed 0.5 percent and silver grades are rarely greater than 0.5 ounce/ton. In contrast, a fissure at the base of Gold Gulch (Plate 1) yielded grades of better than 15 percent combined lead-zinc and 3-4 ounce/ton silver (Martin, personal comm. 1984). Ore occurs as discontinuous high-grade shoots up to five feet thick along the hanging wall of a northwest-trending fault.

Over half of the sulfides in drill cuttings and core occur as disseminations. Disseminated sulfides are found in a variety of structural and stratigraphic settings. Within fractured and silicified zones sulfides are generally fine-grained, randomly dispersed, irregular shaped clots measuring less than two millimeters in diameter. In more porous gouge breccia zones, base-metal sulfides occur as discrete fine-grained euhedral crystals or coarse clots up to two centimeters in diameter (Figure 22). Disseminated base-metals also commonly rim breccia fragments and line vesicles and irregular cavities (Figure 23).

Base-metal sulfide disseminations are generally a combination of two or more intergrown sulfide phases. Pyrite, the most abundant sulfide, is commonly enclosed in sphalerite or galena. Sphalerite commonly rims or replaces galena and locally exhibits a pseudomorphic cubic habit. Chalcopyrite mainly occurs as rounded or rod shaped inclusions in sphalerite and sometimes encloses sphalerite.

Figure 22: Photograph of sphalerite and minor galena lining
irregular shaped vesicles in altered andesite
flow.

Figure 22: Photograph of disseminated sphalerite (brown)
and finer-grained pyrite (brassy) in quartz-
sericite altered andesite.

Tetrahedrite occurs locally as intergrowths with all other sulfides.

Disseminated sulfide zones usually coincide with zones of fracturing and sulfide veining. Veins are generally less than one millimeter thick, occurring along primary joint surfaces or irregular fracture systems. Less commonly, they occur as anastomosing swarms, coarse druses lining open fractures, or as finely laminated "banded" veins.

Veins commonly contain pyrite and locally carry sphalerite, galena, chalcopyrite, covellite, tetrahedrite and arsenopyrite(?). Gangue minerals vary from quartz, clay, calcite, ankerite, rhodochrosite, tourmaline, chlorite, epidote and magnetite. Quartz, tourmaline and clay are most common in rocks showing advanced alteration assemblages; whereas calcite, ankerite, chlorite, magnetite and epidote are generally restricted to propylitic or weak argillic altered zones. Rhodochrosite veining is confined to the upper 50 meters of hole IC-1C.

Core samples commonly show several different stages of fracturing and veining. However, timing and correlation of various different vein episodes is extremely difficult to interpret. In general, there appear to be at least two major stages of quartz-sericite $\pm$ tourmaline $\pm$ pyrite $\pm$ base-metal veining. Many samples in the upper part of IC-1C show a third and possible fourth episode of fracture veining. These latest stages consist of quartz-rhodochrosite-sericite-base-metal veins or drussy quartz-pyrite $\pm$ base-metal veinlets.

Metal Zonation

Geochemical results from four drill holes in the south breccia zone
are illustrated in cross-section in Figures 24 and 25. The most
striking geochemical pattern revealed in these figures is the
coincidence of anomalously high gold, silver, arsenic, lead, and copper
values in several holes which define a zone of metal enrichment
measuring more than 300 meters along section at an average thickness of
60 meters. Intercepts defining this zone are sharply bounded above and
below by relatively barren rock. Transitions between barren and
mineralized rock rarely coincide with abrubt changes in lithology,
sulfide content, vein density or alteration type or intensity (Plate 3).

The distribution of base and precious metals within mineralized
intercepts is relatively consistent throughout most holes. In general,
metal abundances are strongest in the lower parts of individual
intercepts and decrease progressively upwards. Relative increases or
decreases in the abundance of individual elements generally reflect
similar changes in all other metals. However, metal ratios within
intercepts or between holes rarely remain constant.

The highest gold, copper and arsenic values are centered about hole
IC-1R and decrease to the northeast and southwest along section (Figure
24). In contrast, lead and zinc show an overall enrichment to the
northeast (Figure 25). Similarly, the zinc/lead ratio increases in this
direction, varying from .83 in hole IC-1R to 2.35 in hole IC-2R. Silver
has a more erratic distribution; however, it generally correlates with
lead and zinc. The distribution of gold most closely correlates with

SW
NE

IC-5R

IC-2R

Elev.

6100

IC-IR

6000

IC-3R

5900

5800

GEOCHEMISTRY

$\mathcal{\}$ -Au   0 .02 .04 .06

$\mathcal{\}$ -Ag   OPT Au, $\frac{OPT\ Ag}{10}$

5700

$\mathcal{\}$ -As   0 8 16 24 32

PPM As $\times 10^{-2}$

Scale

0   50   100ft.

Vertical Exaggeration = 1.38X
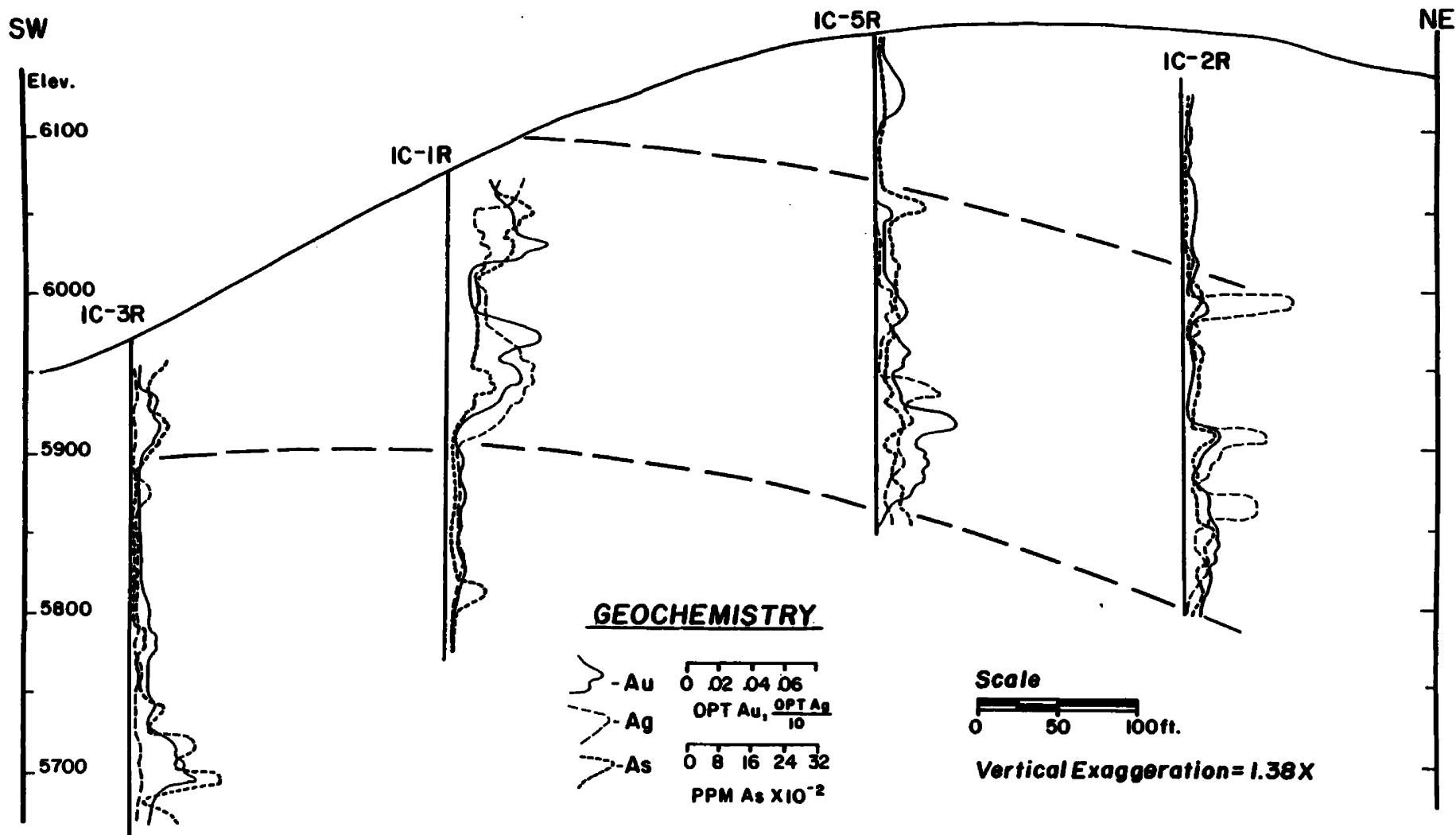
Figure 24. Distribution of Au, Ag, and As in drill holes from the South breccia zone. Heavy dashed lines enclose a zone of combined base and precious metal enrichment. Curves are based on geochemical values averaged over several sample intervals.

54
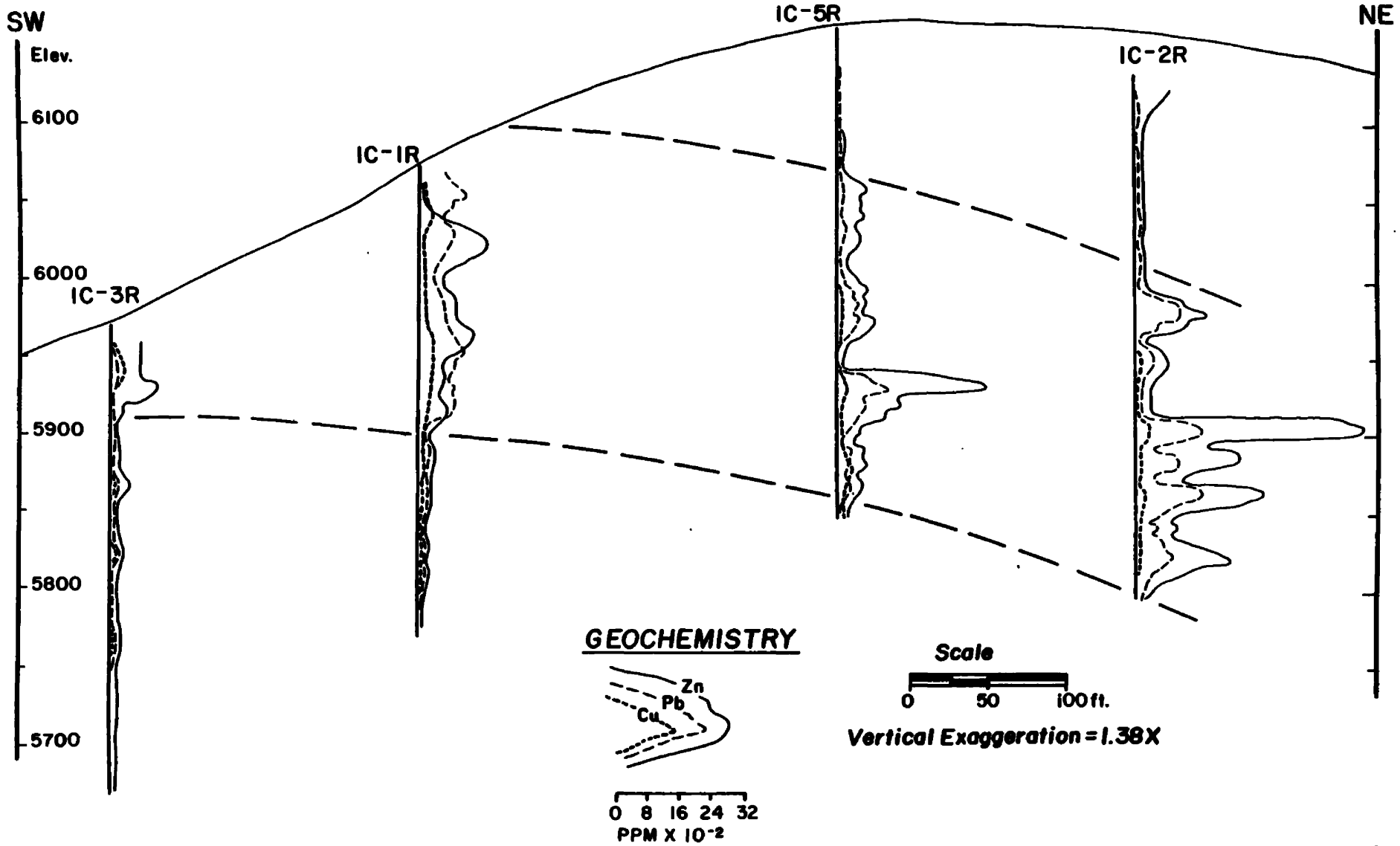
Figure 25. Distribution of Cu, Pb, and Zn in drill holes from the South breccia zone. Heavy dashed lines enclose a zone of combined base and precious metal enrichment. Curves are based on geochemical values averaged over several sample intervals.

arsenic. All intercepts show low gold/silver ratios which vary from .70 in hole IC-3R to .06 in hole IC-2R.

The broad zone of base and precious metal enrichment described above separates two gold-rich zones characterized by a distinct absence of base-metals. The upper zone, which is defined by a 10 meter intercept in hole IC-5R, may correlate with a weak gold anomaly in the upper part of hole IC-2C to the north, and project to the surface to the south. There is a 1:1 correlation between gold and arsenic in the lowermost horizon which is defined by a 40 meter intercept in hole IC-3R. The lateral extent of this mineralized zone has not been drill tested.

Fluid Inclusions

Procedures

Several samples were selected for fluid inclusion analysis to determine the thermochemical characteristics of the hydrothermal system. The study was limited to vein sets from both core holes and surface exposures in the south breccia zone. Much of the data discussed in this section was generated by Reynolds (1983). All measurements were taken from inclusions within quartz.

Thin (<150 microns) doubly-polished plates were surveyed at the onset of the study to locate inclusions conducive to analysis. Fluid inclusion types, kinds, sizes, and relative abundances were recorded for all samples. Temperature and salinity determinations were made on seven samples using a Fluid, Inc. adapted U.S. Geological Survey gas-flow

heating/freezing system which operates by passing preheated or cooled N2 gas directly over the sample. Homogenization temperatures are accurate within one percent of the measured values except for vapor-rich inclusions ($\pm$15C). Freezing tests are accurate within 3C. Fluid inclusions were subjected to heating tests prior to freezing to prevent cracking and leakage.

Fluid inclusions were classified on the basis of phases observable at room temperature according to methods described by Nash (1976). Two phase inclusions containing less vapor than liquid are referred to as Type I inclusions and homogenize by the disappearance of the vapor phase. Type II inclusions contain greater than 50 volume percent vapor and homogenize by expansion of the vapor phase. Inclusions which contain halite in addition to liquid and vapor phases are considered Type III inclusions. Homogenization temperatures for Type III inclusions correspond to the temperature of vapor bubble disappearance or dissolution of halite, whichever is higher.

Salinities were calculated for Type I inclusions from freezing data by the method of Potter and others (1978). Salinities for Type III inclusions were calculated by applying temperatures of halite dissolution to equations in Potter and others (1977). All salinities are reported in weight percent NaCl equivalent.

Classification of inclusions as primary, secondary and pseudosecondary (Roedder, 1981) were made when possible. However, in most samples the presence of abundant randomly oriented planes of fluid inclusions made determinations difficult.

General Observations

Abundant fluid inclusions occur throughout all samples examined; however, those having properties suitable for analysis were generally rare. Heating and freezing tests were hampered by the small sizes of most inclusions and poor resolution of most polished sections. Inclusions were generally less than 10 microns in diameter but locally measured up to 45 microns. Most of the data in this study was taken from inclusions ranging from three to 15 microns.

Three different types of inclusions were recognized. By far, the most abundant were vapor-rich (Type II) inclusions which comprise greater than 80 percent of all inclusions observed. Vapor-rich inclusions generally contain little to no liquid at room conditions. The lack of liquid in most Type II inclusions made heating/freezing tests very difficult, if not impossible.

Vapor-rich inclusions described above always coexist with liquid-rich (Type I) inclusions, except in some late stage quartz-pyrite microveinlets (samples IC-108.5, IC-120.3 and IC-146) which contain only Type I inclusions (Reynolds, 1983). Although Type I inclusions comprise less than 15 percent of all inclusions observed, they were the source of most heating/freezing data collected. These inclusions contain variable amounts of vapor; generally less than 15 volume percent, but range up to 40 volume percent.

The third type of inclusion (Type III) observed contained a halite daughter mineral in addition to liquid and vapor phases. Halite was recognized by its isotropic character and cubic habit. Type III

inclusions are generally rare; however, they occur in many samples surveyed and are abundant in at least one (sample 1018-4). Most Type III inclusions homogenized by dissolution of halite prior to disappearance of the vapor phase.

Temperature and Salinity

Figure 26 combines fluid inclusion data obtained from seven different vein samples collected from core holes and surface exposures in the south breccia zone. Combined results for all inclusions reveal a wide variability in fluid temperatures and salinities. Homogenization temperatures ranged from 170C to greater than 550C, and salinities varied from 0.87 to 47 weight percent NaCl equivalent. Despite this extreme variability, most inclusions fall within two distinct temperature/salinity fields.

The majority of all inclusions surveyed had low to moderate salinities (0.87 to 16 weight percent NaCl equivalent), and homogenized at temperatures ranging from 240C to 380C. This group is characterized by abundant liquid- and vapor-rich inclusions which are somewhat lower temperature than a second group of hypersaline inclusions. This second group of inclusions homogenized at temperatures ranging from 300C to greater than 550C and had salinities varying from 31 to 47 weight percent NaCl equivalent.

The conspicuous absence of salinity measurements (16 to 31 weight percent NaCl equivalent) between the above two groups does not appear to be a result of leakage, necking down, or mixed-phase entrapment. Had
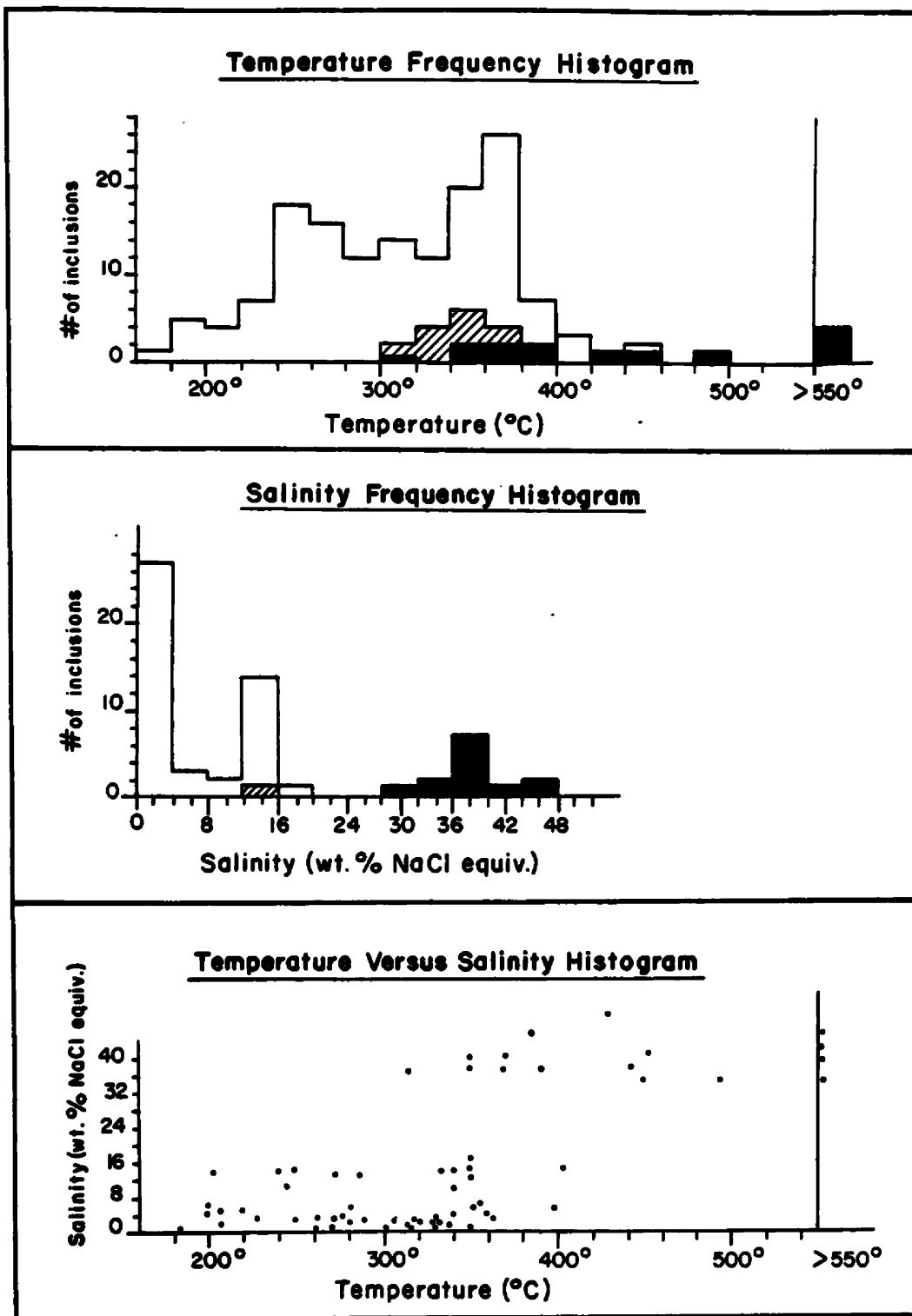
Figure 26: Frequency histograms showing combined temperature and salinity results for Type I (open), Type II (hachured), and Type III (solid) fluid inclusions from seven vein samples. Individual results are given in Appendix C.

these processes occurred, one would expect a continuum between low and high salinity inclusions (Reynolds, 1980). Furthermore, the gap is not believed to be a function of measurement error or insufficient data based on the abundance of salinity measurements which occur just above and below this break. Similar bimodal distributions of salinity values in most porphyry systems have been attributed to two distinctly different hydrothermal fluids (Nash, 1976; Bodnar and Beane, 1980).

Temporal Variations in Fluid Chemistry

Temporal variations in fluid chemistry and temperature were determined by comparing fluid inclusion results for several different veins. Figure 27A-L gives heating/freezing results for quartz ± tourmaline-base-metal veins in both core holes (samples 1C-108.5 and 2C-199.8), a quartz-sericite-pyrite veinlet (surface sample 1018-4), and quartz associated with a late-stage tourmaline breccia dike (surface sample IC-40). Fluid inclusion results for several other veins are given in Appendix C.

Comparison of temperature/salinity results for quartz-tourmaline-base-metal veinlets from both drill holes revealed remarkable similarities (Figure 27D-I). Both are characterized by abundant low to moderate salinity Type I and Type II inclusions which homogenize at temperatures ranging from 240C to about 380C. In contrast, the quartz-sericite-pyrite veinlet contains abundant hypersaline inclusions which homogenize at somewhat higher temperatures (300C to >550C), in addition to abundant liquid- and vapor-rich
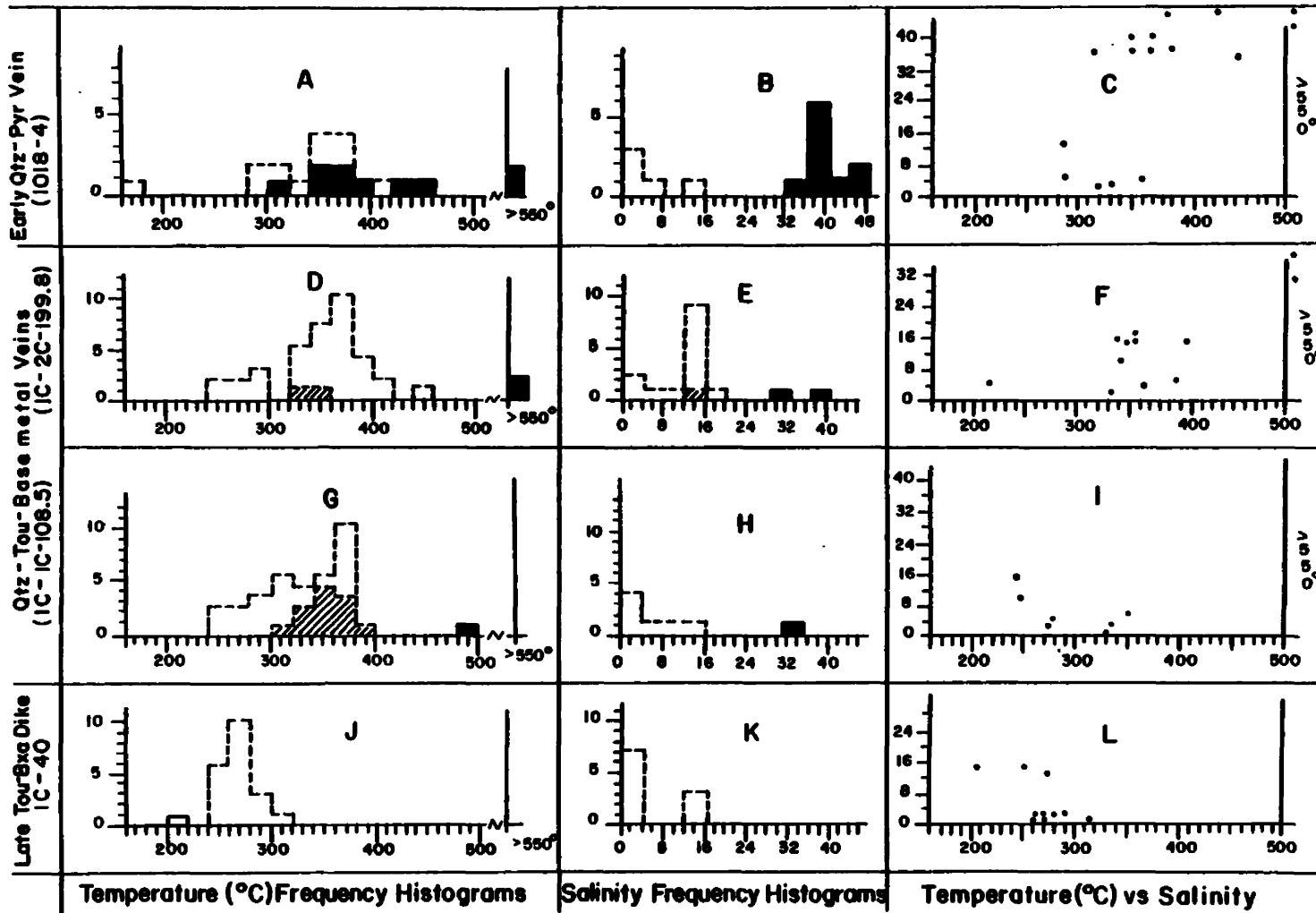
Figure 27: Frequency histogram showing homogenization temperatures and salinities for Type I (open), Type II (hachured), and Type III (solid) fluid inclusions from three different stages of veining. Salinity given in weight-percent NaCl equivalent.

Temperature (°C) Frequency Histograms   Salinity Frequency Histograms   Temperature(°C) vs Salinity

Early Qtz-Pyr Vein (1018-4)

Qtz-Tou-Base metal Veins (IC-2C-199.8)

Qtz-Tou-Base (IC-IC-108.5)

Late Tour-Bxa Dike IC-40

inclusions comparable in salinity and temperature to quartz-tourmaline .

veinlets (Figure 27A-C). The apparent overlap in salinity and

temperature data in both vein types (quartz-tourmaline and

quartz-sericite) suggests the quartz-tourmaline episode is superimposed

on the quartz-sericite-pyrite vein. Furthermore, the paucity of Type

III inclusions in quartz-tourmaline veinlets suggests the

higher-temperature, hypersaline veins (1018-4) are probably older.

Heating and freezing tests on a late-stage tourmaline breccia dike

yielded temperatures generally in the range of 240C to 300C and low to

moderate salinities (Figure 27J-L). This dike (IC-40) cross-cuts an

earlier stage of quartz and minor tourmaline alteration (Figure 15)

which may be equivalent to the quartz-base-metal stage.

A later, lower temperature episode of veining was observed in a

number of samples (Appendix C). This stage is most obvious in sample

108.5, where quartz-pyrite microveinlets, characterized by abundant Type

I inclusions homogenizing between 220C and 260C offset the

quartz-tourmaline-base-metal veinlet discussed earlier.

In summary, there appears to be a direct relationship between

quartz-tourmaline-base-metal veins in both core holes. These veins are

characterized by abundant low-moderate salinity Type I and II inclusions

which homogenize at temperatures ranging from about 300C to 380C.

Quartz-base-metal veining was followed by a lower temperature

quartz-tourmaline stage characterized by abundant vapor-rich inclusions.

These episodes of veining may post-date filling of a

quartz-sericite-pyrite vein characterized by high temperature,

hypersaline inclusions. The youngest episode is characterized by lower temperature quartz-sulfide veins containing abundant Type I inclusions.

DISCUSSION

Depositional Environment

The development of breccia zones at Idol City is clearly related to the hydrothermal process. In addition to being centers of alteration and mineralization, the following breccia textures link the origin of breccias to the hydrothermal event:

1. fragments are remnants of earlier episodes of alteration
   and veining,

2. fragments of different alteration types occur within a
   single hand sample, and

3. veining within fragments is truncated by a hydrothermal
   matrix of different alteration assemblages.

Mechanisms which could account for a syn-mineralization-brecciation event include: chemical or solution brecciation (Sawkins, 1969), explosive action of superheated water into vapor (Berger and Eimon, 1982), or opening of multiplane faults (Mitcham, 1974). Although all three mechanisms could account for the above described textures, faulting and chemical brecciation have definite shortcomings.

Faulting typically does not show the type or degree of fragment transport as is indicated by mixing, rounding, size grading or alignment of fragments observed in many tourmaline breccia samples. Additionally,

faulting could not account for the distribution of tourmaline breccia dikelets which have discrete contacts with surrounding wallrocks.

Chemical brecciation is inconsistent with alteration suites exhibited by both breccia zones. Abundant sericite and kaolinite throughout breccias reflect wall-rock interaction with fluids having a relatively low pH and high cation/H ion concentration (Hemley and Jones, 1964). Such fluids would be incapable of dissolving andesitic rocks.

Many analogies can be made between the character and distribution of breccias at Idol City with hydrothermal explosion breccias documented elsewhere. Features considered diagnostic of an explosive hydrothermal origin in porphyry related deposits are given below for comparison (Table 3). Similar characteristics are used as permissive evidence of an explosive origin in epithermal systems (Berger and Eimon, 1982; and Giles and Nelson, 1982).

Table 3. Diagnostic Features of Hydrothermal Breccias
        (after Sherkenback, 1982)

1. Irregular to pipe-like shape.

2. Common associations of breccias with faults or intrusions.

3. Widespread size range and angularity of fragments.

4. Upward and/or downward movement of fragments in a breccia body.

5. Downward termination of brecciation into larger fragments of rock that have moved progressively smaller distances.

As previously mentioned, tourmaline breccias at Idol City exhibit most of the above characteristics. Breccia fragments show all degrees of size, sorting, angularity, and cementation. Fragment transport is indicated by the strong preferred orientation of tabular clasts, size grading of rounded clasts, and mixing of clasts of different lithologies and alteration types.

Additionally, breccias are spatially associated with felsic intrusions, occurring as isolated pipe- and dike-like features elongate in a southwest-northeast direction. The northeast trend of both breccia zones is probably fault related judging from the abundance of gouge-cemented rubble encountered in several drill holes.

Hydrothermal breccias have recent analogs in active geothermal systems. Explosive hydrothermal activity has been documented in Yellowstone National Park, Wyoming (Muffler and Truesdell, 1971), Steamboat Springs, Nevada (White, 1981), and several geothermal fields in the Taupo volcanic zone of New Zealand (Henley and Hedenquist, 1983). It occurs when the vapor pressure of water exceeds lithostatic load plus the tensile strength of enclosing rocks (Henley and McNabb, 1978). Drilling in Yellowstone Park established the existence of fluid pressures in excess of 30% above hydrostatic (White and others, 1983). Fluid over-pressuring in this and other geothermal systems has been attributed to silica sealing of major outflow structures. Breccia clasts are commonly remnants of earlier episodes of hydraulic fracturing and self-sealing (Berger and Eimon, 1982).

Boiling as a mechanism of Ore Deposition

Fluid inclusion data suggests that Idol City fluids experienced episodic boiling events. Boiling commonly occurs in response to rapid drops in pressure triggered by explosive hydrothermal activity or due to the rise of superheated fluids into lower pressure regions (Cunningham,1978).

Boiling is suggested in base-metal veins by the coincidence of liquid- and vapor-rich inclusions which homogenize at similar temperatures (Figures 27D and G). This observation coupled with the fact that most inclusions seen in these veins were vapor-rich is permissive evidence that boiling occurred (Roedder, 1981). At lower temperatures, 240C to 300C, abundant liquid- and vapor-rich inclusions also coexist; however, none of the vapor-rich inclusions would homogenize. Reynolds (1982) suggests that vapor-rich inclusions formed during boiling at temperatures below 300C do not homogenize due to a lack of liquid trapped at the two-phase (liquid-vapor) boundary. Boiling is also indicated in this low temperature range by the presence of explosive brecciation textures in many rocks.

Boiling could account for the wide variability in homogenization temperatures for quartz-base-metal veins (300C-380C) and tourmaline breccias (240C-300C). According to Reynolds (1983), fluid inclusions formed during boiling rarely trap a homogenous liquid or vapor. Small amounts of liquid are often trapped with steam and minor vapor is trapped with liquid, thus yielding homogenization temperatures higher than trapping temperatures. In theory, the lowest temperature

determined from a large population of inclusions formed during boiling should represent the true trapping temperature (Reynolds, 1983). Thus, the broad variability in temperature data for base-metal veining and tourmaline brecciation may reflect boiling at temperatures ranging from 240C to 300C.

Boiling could also explain the variability in salinity measurements (0.8-16.0 weight % NaCl equiv.) in most moderate temperature veins (Figure 27E and H). Changes in salinity commonly occur in response to entrapment of fluids with different densities from a progressively boiling hydrothermal system (Cunningham, 1978). These changes are reflected by the presence of sericite and kaolinite throughout both breccia zones. Selective partitioning of H2S and HCl into the vapor phase during boiling would produce acid conditions on condensation capable of forming kaolinite, while alkali-rich residual liquid could simultaneously form sericite (Hemley and Jones, 1964).

Boiling promotes deposition of metals by partitioning volatiles into the vapor phase and thus changing the solubility of metal complexes (Drummond, 1981). Loss of CO2, H2S, or HCl into the vapor phase can cause changes in pH, composition, ionic strength and oxygen fugacity of the remaining fluids; thus causing ore and gangue minerals to precipitate.

Pressure release and resultant boiling could also drastically decrease the temperature of the remaining fluid (Cunningham, 1978). For example, the transition between lithostatic and hydrostatic pressures at depths of less than 1000 meters can produce a sudden drop in fluid

temperature of more than 80C (Figure 28). Such changes in temperature significantly affect the solubility of metal complexes. Kay and Strong (1983) noted an almost exponential decrease in gold solubility between temperatures of 300C-400C.

Depth of Mineralization

Depth at which various stages of veining took place can be estimated from temperature and salinity results for fluids interpreted as having undergone boiling (Roedder and Bodnar, 1980). According to Figure 28 , boiling of low-moderate salinity fluids at about 300C would occur at depths less than 1100 meters under hydrostatic conditions and 315 meters under lithostatic load. In contrast, lower temperature veining associated with boiling at 240C would take place at depths less than 380 meters or 140 meters assuming hydrostatic or lithostatic conditions, respectively.

Magmatic Input

Several lines of evidence suggest felsic intrusions may be geneticly related to the ore forming process. Although rhyolite and quartz-porphyry intrusions are rarely mineralized they commonly exhibit alteration halos similar to those present in ore zones. Additionally, a radiometric age determination of 21.+.9 m.y. on a rhyolite dike in the north part of the map area is close to a date of 19+.8 m.y. for sericite alteration in the south breccia (Appendix B).
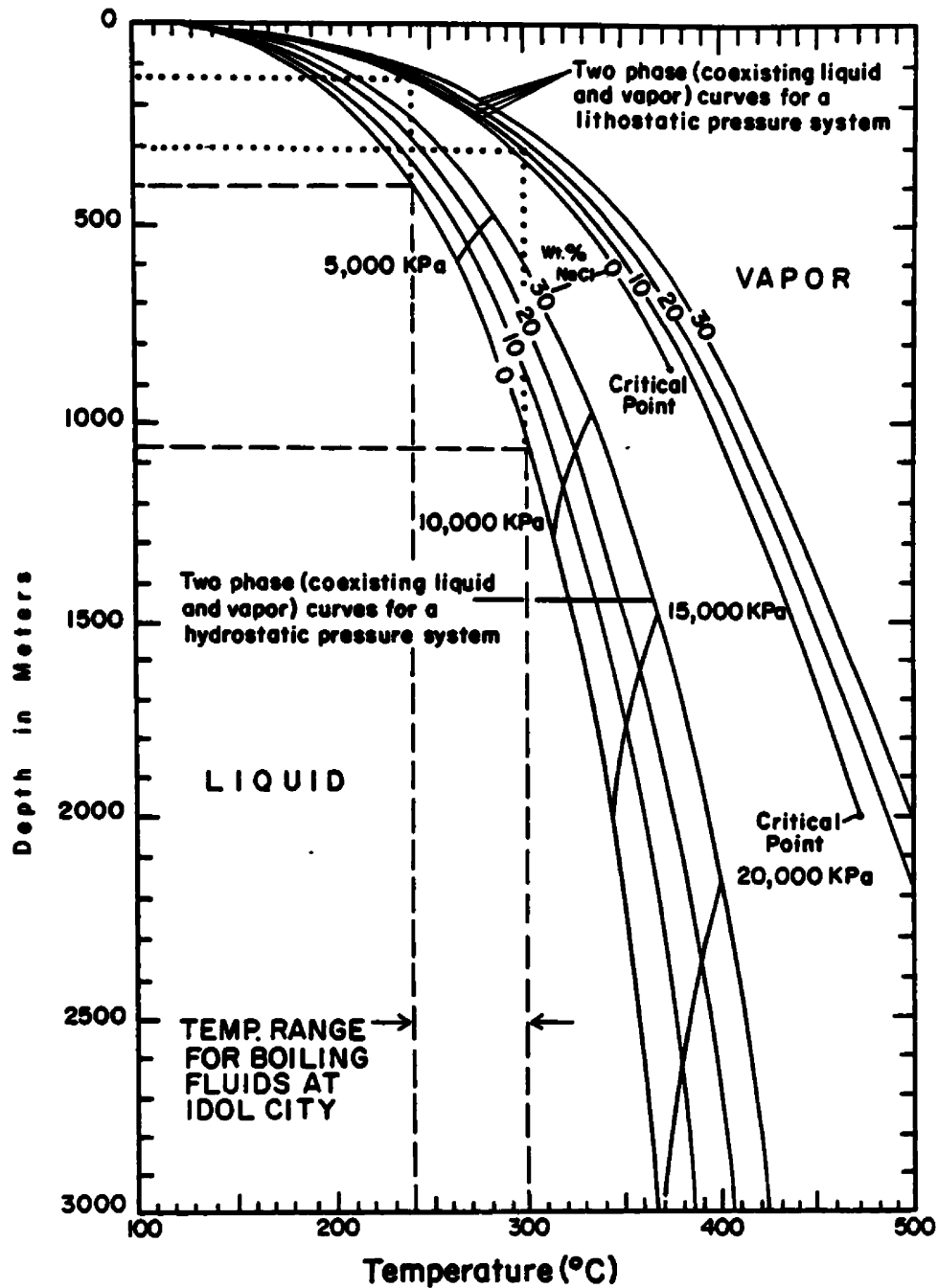
Figure 28: Temperature-pressure-depth diagram of the two-phase boundaries in the H_2O-NaCl system (modified from Haas, 1971, 1976; Sourirajan and Kennedy, 1962). Note the slope of two-phase (boiling) curves flattens markedly at shallow depths. Thus, a change in pressure at shallow depths is much more likely to cause boiling than at greater depths. Dashed and solid lines indicate depths of boiling at Idol City assuming hydrostatic or lithostatic conditions, respectively.

The influence of intrusive activity is also indicated by fluid inclusion data. The presence of highly saline (>35wt% NaCl eq.) inclusions in some samples is considered by many as strong evidence that fluids trapped derivatives of a crystallizing melt (Reynolds, 1984). The fact that some fluids were trapped at temperatures in excess of 550C also supports a magmatic source.

Genetic Model

Mineralization resulted from a complex interplay of tectonic, magmatic, and hydrothermal events (Figure 29). Northeast and northwest trending faults occurred early in the evolution of the Idol City system and became the locus for hydrothermal activity. Faulting provided access for deep circulation of mineralizing waters and focused deep system fluids into the surface depositional environment. These fluids may have eventually vented in the form of hot-springs or geysers. The absence, however, of near-surface features such as low temperature quartz or zones of intense acid leaching suggest altered and mineralized rocks exposed at Idol City represent a deeper level of exposure within the proposed geothermal system (Figure 29).

Physical, chemical, and fluid inclusion data indicate deposition of disseminated base and precious metals occurred in response to boiling. Drastic chemical and temperature changes accompanying boiling are sufficient to cause ore and gangue minerals to precipitate (Drummond, 1981).
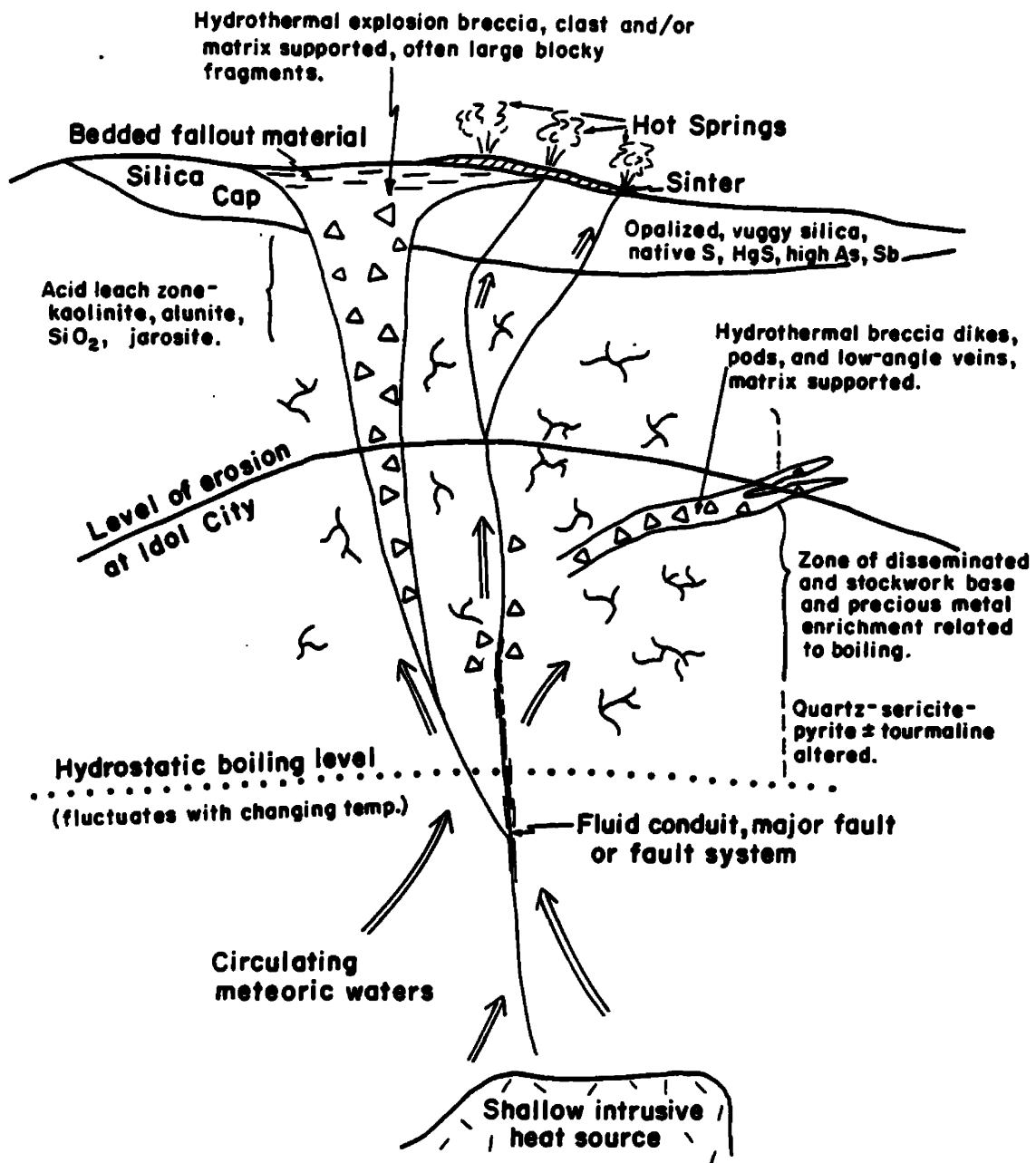
Figure 28: Genetic model for disseminated/stockwork mineralization at Idol City. Modified after near-surface hot-spring model of Berger and Eimon (1982). Note level of erosion at Idol City.

The distribution of hydrothermal breccia on the surface and in drill holes suggests that boiling resulted from the explosive release of over-pressured fluids. Silicified and tourmalinized zones acted as impermeable barriers, restricting the flow of mineralizing solutions and promoting fluid over-pressuring. The sudden release of pressure accompanying the rupture of silicic cap rocks would result in retrograde boiling to significant depths. Periodic rupturing and self sealing is evidenced by multiple episodes of brecciation, fracturing, and veining.

The apparant lateral and vertical continuity of mineralizaiton in the south breccia zone suggests that deposition occurred at a relatively shallow depth where steep environmental gradients prevail (Cunningham, 1978). Figure 28 shows how minor fluctuations in temperature and pressure can result in boiling at shallow depths. Boiling temperatures of approximately 300C for base-metal stockworks indicate that deposition of metals could have occurred at depths as shallow as 315 meters accompanying a drop in pressure from lithostatic to hydrostatic conditions.

Felsic intrusions are spatially, temporally, and probably geneticaly related to the ore forming process. Intrusive activity could account for the heat required to sustain long periods of convective hydrothermal activity.

REFERENCES CITED

Allen, J.E. and Bealieu, J.D., 1976; Plate Tectonic Structures in
    Oregon: The Ore Bin, vol. 38, no. 6, p. 87-99.

Beane, R.E. and Titley: 75th Ann. Vol. Econ. Geol.

Beauliew, J.D. 1972; Geologic formations of eastern Oregon (east of
    longitude 12130´): State of Ore. Dept. of Geol. and
    Min. Ind. Bull. 73, 79 p.

Berger, B.R. and Eimon, P.I., 1982; Comparative models of epithermal
    silver-gold deposits: SME-AIME Ann. Mtg., Feb. 1982, Pre-print
    82-13, 25 p.

Bodnar, R.J. and Beane, R.E., 1980; Temporal and spatial variations in
    hydrothermal fluid characteristics during vein filling in pre-ore
    overlying deeply-buried porphyry copper mineralization at Red
    Mountain, Arizona: Econ. Geol., vol. _, p. 876-893.

Brown, C.E. and Thayer, T.P., 1966; Geologic map of the Canyon City
    quadrangle, northeastern Oregon: U.S. Geol. Survey
    Misc. Geol. Inv. Map I-447, scale 1:250,000.

Buchanon, L.J., 1981; Precious metal deposits associated with volcanic
    environments in the southwest, in Dickinson, W.R. and Payne, W.D.,
    eds., Relations of tectonics to Ore Deposits in the Southern
    Cordillera: Ariz. Geol. Soc Digest, vol. 14, p. 237-262.

Christiansen, R.L. and Lipman, P.W., 1972; Cenozoic volcanism and
    plate-tectonic evolution of the western United States: II. Late
    Cenozoic: Phil. Trans. R. Soc. Lond. A. 271, p. 249-284.

Cunningham, C.G., 1978; Pressure gradients and boiling as mechanisms
    for localyzing ore in porphyry systems: Jour. Research
    U.S. Geol. Survey, vol. 6, no. 6, p. 745-754.

Davie, E.I., Leavitt, J.D. and Howell, R.L., 1980; Summary report of
1980 Oregon Tertiary Au-Ag reconnaissance: Unpublished Noranda
Exploration, Inc. company report, p. 5-10.

Dicken, S.N., 1950; Oregon (1st ed.): Ann Arbor, Mich. Edward Bros.,
Inc., 104 p.

Drummond, S.E., 1981; Boiling and mixing of hydrothermal fluids:
Chemical effects on mineral precipitation: PhD Dissertation,
Pennsylvania State Univ., 380 p.

Enlows, H.E., 1976; Petrography of the Rattlesnake formation at the
type area, central Oregon: Oregon Dept. of Geol. and
Min. Ind. Short Paper 25, 34 p.

Greene, R.C., 1973; Petrology of the welded tuff of Devine Canyon,
southeastern Oregon: U.S.G.S. Prof. Paper 797, 26 p.

_____, Walker, G.W. and Corcoran, R.E., 1972; Geologic map of the
Burns quadrangle, Oregon: U.S. Geol. Survey Misc. Geol. Invest.
Map I-680, scale 1:250,000.

Giles, D.L. and Nelson, C.E., 1982; Principle features of epithermal
lode gold deposits of the circum-Pacific rim: Presented at
Circum-Pacific Energy and Min. Res. Conf., Honolulu, Hawaii.

Haas, J.L., 1971; The effect of salinity on the maximum thermal
gradient of a hydrothermal system at hydrostatic pressure:
Econ. Geol., vol. 66, no. 6, p. 940-946.

_____, 1976; Thermodynamic properties of the coexisting phases and
thermodynamic properties of the NaCl component in boiling NaCl
solutions: U.S. Geol. Survey Bull. 1421-B, 71 p.

Hemley, J. and Jones, W., 1964; Chemical aspects of hydrothermal
alteration with emphasis on hydrogen metasomatism: Econ. Geol.,
vol. 59, p. 538-569.

Henley, R.W. and McNabb, A., 1978; Magmatic vapor plumes and
     ground-water interaction in porphyry copper emplacement:
     Econ. Geol., vol. 73, no. 1, p. 1-20.

_____ and Hedenquist, J.W., 1983; An introduction to the geochemistry
     of active and fossil geothermal systems: Presented at Epithermal
     Environments in New Zealand Field Conf., Feb. 13-20, 1983.

Kay, A. and Strong, D.F., 1983; Geologic and fluid controls on As-Sb-Au
     mineralization in the Moretons Harbour area, Newfoundland:
     Econ. Geol., vol. 78, p. 1590-1604.

Kittleman, L.R., Green, A.R., Johnson, A.M., McMurray, J.M., Russell,
     R.G. and Weeden, D.A., 1965; Cenozoic stratigraphy of the Owyhee
     region, southeastern Oregon: Univ. of Ore., Museum of Natural
     History Bull. 1, 45 p.

Kubler, B., 1968; Evaluation quantitative du metamorphisme par la
     cristallinite de l'illite: Centre de Reserches de Pau - S.N.P.A.,
     Bull. 2, p. 385-397.

Lawrence, R.D., 1976; Strike-slip faulting terminates the Basin and
     Range province in Oregon: Geol. Soc. Am. Bull., vol. 87,
     p. 846-850.

Leavitt, J.D., 1981; Summary report of Idol City prospect: Unpublished
     Noranda Exploration, Inc. company report, 18 p.

Lipman, P.W., Prostka, H.J. and Christiansen, R.L., 1972; Cenozoic
     volcanism and plate-tectonic evolution of the western United
     States: I. Early and middle Cenozoic:
     Phil. Trans. R. Soc. Lond. A. 271, p. 217-248.

MacLeod, N.S., Walker, G.W. and McKee, E.H., 1975; Geothermal
     significance of eastward increase in age of upper Cenozoic rhyolite
     domes in southeastern Oregon: U.S.G.S. Open-File Report 75-348, 22
     p.

Martin, H., 1984; Personal communicaiton: Property owner - Idol City
     area, Petaluma, California.

McGrane, D.J., 1982; Summary report of the 1982 Idol City project:
Unpublished Noranda Exploration, Inc. company report, 21 p.

_____, 1983; Summary report of the 1983 Idol City project:
Unpublished Noranda Exploration, Inc. company report, 21 p.

_____, 1984; Idol City project final report: Unpublished Noranda
Exploration, Inc. company reprot, 28 p.

Mitchel, M.J., 1962; Idol City mine, Harney County, Oregon:
Unpublished geologic and economic evaluation, 6 p.

Mitchem, T.W., 1974; Origin of breccia pipes: Econ. Geol., vol. 69,
p. 412-413.

Muffler, L. and Truesdall, A., 1971; Hydrothermal explosion craters in
Yellowstone National Park: Geol. Soc. Am. Bull., vol. 82,
p. 723-740.

Nash J.T., 1976; Fluid-inclusion petrology - Data from porphyry copper
deposits and applications to exploration: U.S. Geol. Survey
Prof. Paper 907-D, 16 p.

Parks, H.M. and Swartley, A.M., 1961; Handbook of the Mining Industry
of Oregon (alphabetical list if properties; description of mining
districts): Min. Res. of Oregon Bur. Mines and Geol., vol. 2,
no. 4, 306 p.

Potter, R.W., Jr., Babcock, R.S. and Brown, D.L., 1977; A new method
for determining the solubility of salts in aqueous solutions at
elevated temperatures: Jour. Res. U.S. Geol. Survey, vol. 5,
p. 389-395.

_____, Clynne, M.A. and Brown, D.L., 1978; Freezing point depression
of aqueous sodium chloride solutions: Econ. Geol., vol. 73,
p. 284-285.

Reynolds, T.J., 1980; Variations in hydrothermal fluid characteristics through time at the Santa Rita porphyry copper deposit, New Mexico: M.S. Thesis, Univ. of Arizona, 52 p.

_____, 1983; Short course on fluid inclusions: A two day seminar presented at the Univ. of Montana.

_____, 1984; Fluid Inclusion Study of various gold deposits and prospects for Noranda Exploration Inc. projects: Unpublished Noranda Exploration, Inc. report.

Robyn, T.L., 1979; Miocene volcanism in eastern Oregon: An example of calc-alkaline volcnism unrelated to subduction: Jour. Vol. and Geotherm. Res., vol. 5, p. 149-161.

Roedder, E. and Bodnar, R.J., 1980; Geologic pressure determinations from fluid inclusion studies: Ann. Earth Planet. Sci., vol. 8, p. 263-301.

_____, 1981; Origin of fluid inclusions and changes that occur after trapping: In Min. Assoc. of Canada Short Course Handbook, vol. 6, p. 101-135.

Sawkins, F.J., 1969; Chemical brecciation, an unrecognized mechanism for breccia formation: Econ. Geol., vol. 64, pl 613-617.

Sherkenback, D.A., 1982; Geologic, mineralogic, fluid inclusion and geochemical studies of the mineralized breccias at Cumobabi, Sonora, Mexico: PhD Dissertation, University of Minnesota, 190 p.

Sourirajan, S. and Kennedy, G.C., 1982; The system H2O-NaCl at elevated temperatures and pressures: Am. Jour. Sci., vol. 260, p. 115-141.

Swanson, D.A. and Robinson, P.T., 1968; Base of the John Day formation in and near the Horse Heaven mining district, north-central Oregon: U.S.G.S. Prof. Paper 600-D, p. 154-161.

Thayer, T.P., 1969; Geology of the Blue Mountain region in Mineral and Water Resources of Oregon: State of Ore. Dept. of Geol. and Min. Ind. Bull. 64, p. 68-73.

Thompson, G., 1983; Personal communication: Clay mineralogy instructor, Univ. of Montana.

Walker, G.W., 1969a; Geology of the High Lava Plains province in Mineral and Water Resources of Oregon: State of Ore. Dept. of Geol. and Min. Ind. Bull. 64, p. 74-83.

_____, 1969b; Geology of the Basin and Range province in Mineral and Water Resources of Oregon: State of Ore. Dept. of Geol. and Min. Ind. Bull. 64, p. 83-88.

_____, 1977; Geologic map of Oregon east of the 121st meridian: U.S.G.S.3Misc. Invest. Series Map I-902, scale 1:500,000.

_____, 1979; Revisions to the Cenozoic stratigraphy of Harney Basin, southeastern Oregon: U.S.G.S. Bull. 1475, 35 p.

White, D.E., 1981; Active geothermal systems and hydrothermal ore deposits: Econ. Geol., 75th Anniversary Vol., p. 392-423.

_____ and Heropoulos, C., 1983; Active fossil hydrothermal-convection systems of the Great Basin: Presented at Geothermal Resources Council Proceedings, Reno, Nevada.

Young, P.C., 1983; Panned concentrates from reverse-circulation-drill hole IC-1R, Idol City project: Unpublished Noranda Exploration, Inc. interoffice memo.

APPENDIX A. Petrographic Features of Analyzed Rocks

1027-10   Aphyric basalt - comprised of a dense ophitic intergrowth of subhedral augite (45%) measuring up to 1mm enclosing finer-grained ($\leq$.3mm) plagioclase laths. Local plagioclase phenocrysts up to 1.5mm, minor intergranular olivine (2%) and magnetite (2%), intersertal glass. Glass locally altered to chlorite. Minor vesicles up to 1mm.

814-1   Porphyritic basalt - comprised of 5% subhedral plagioclase phenocrysts up to 3.5mm in length set in a randomly oriented intergrowth of plagioclase microlites (60%),augite 7-10%, olivine (10%) and opaque oxides (1-2%) measuring <.5mm. Contains minor intersertal glass.

1029-9   Two pyroxene andesite - comprised of 6% combined hypersthene and augite measuring up to 1.5mm in length and 15% plagioclase (1.0-2.5mm in length). Phenocrysts and glomerocrysts set in a plagioclase microlite (10%) and glass groundmass. Large plagioclase phenocryst are strongly resorbed exhibiting sieve textures, whereas smaller grains are fresher and commonly zoned.

1013-3   Two pyroxene andesite - comprised of hypersthene (3%) and augite (1-2%) measuring up to 1mm in length and 30-35% plagioclase phenocrysts (1-2.5mm in length) in a plagioclase microlite (5%) and glass groundmass. Pyroxenes are locally rounded and resorbed, replaced by minor calcite and rimmed by iron-oxides. Larger plagioclase exhibit sieve textures.

1018-1   Two pyroxene andesite - comprised of 15% plagioclase (.5-3.0mm, commonly zoned), 2-3% augite up to 2mm in length, 1-2% hypersthene ($\leq$1.5mm) phenocrysts and glomerocrysts in a crowded pilotaxitic plagioclase (45%, $\leq$.2mm) groundmass containing up to 30% intersertal glass. Plagioclase is commonly strongly zoned and locally contains poikyolitic intergrowths of hypersthene. Augite is locally embayed by hypersthene. Minor vesicles are present up to 1mm diameter.

1029-3　　Two pyroxene andesite – comprosed of 25% plagioclase up to 2mm in length and 7% combined intergranular hypersthene and augite in a very fine-grained quartz, chlorite, calcite, magnetite, clay altered groundmass. Contains ovoid vesicles up to 1.5mm diameter concentricly zoned with magnetite, epidote, quartz and calcite toward the core. Feldspars are locally replaced by similar alteration minerals.

725-1　　Hornblende andesite – comprised of 8% plagioclase, 4-5% horblende and 1-2% chloritized pyroxene phenocrysts up to 2mm in length. Groundmass consists of intergranular plagioclase, quartz, calcite and opaque oxides with intersertal glass. Hornblende locally forms poikyolitic intergrowths in plagioclase. Plagioclase phenocrysts are generally well zoned, strongly resorbed and sieve textured.

1212-1　　Hornblende andesite – comprised of 15% plagioclase (<2.5mm) phenocryst and intergranular hornblende (3-4%) and biotite (<1%) up to 1mm set in a pilotaxitic plagioclase groundmass with minor intersertal glass. Coarse hornblende, plagioclase, biotite glomerocrysts are common. Calcite and makes up about 7-10% of sample; locally replacing hornblende, plagioclase, and glass.

1017-5　　Hornblende andesite – comprised of 7% plagioclase phenocryst up to 2.5mm and 3-4% hornblende phenocrysts measuring up to 1.5mm set in a pilotaxitic plagioclase microlite (60%) groundmass. Groundmass containing minor intersertal glass. Contains approximately 3% epidote and 4% calcite as alterations of hornblende and plagioclase.

1028-1　　Hornblende andesite – comprised of 5-7% plagioclase phenocryst measuring 1.0-3.5mm and 7% chlorite and calcite altered hornblende (<1mm diameter) set in a pilotaxitic plagioclase (60%, <.5mm), magnetite (2%), glass groundmass. Feldspar phenocrysts are locally altered to clay and commonly calcite replaced along crystal faces and fractures.

APPENDIX B. Potassium-Argon Age Determinations

Procedures

Age determinations for two samples were made by Krueger Enterprises, Inc., Cambridge, Mass. on February 10, 1984. Determinations on both samples were given for mineral seperates. Rocks were crushed, washed, and sieved to -80/+200 mesh size. Sanidine from sample 1019-5 was separated magnetically, treated with dilute acid to remove slight alterations and glass, and sunk in heavy liquids to remove quartz. Sericite from sample IC-2C-423′ was separated by a series of magnetic concentrations with a final heavy liquid sink.

Potassium was determined by flame photometry. Argon extractions were made by induction heating in high vacuum pyrex extration lines using istotope dilutions techniques. Air argon averages about 1.5 percent in sample IC-2C-423′ and 2.2 percent in sample 1019-5 using the equation: air /argon=(1-Ar40*/total Ar40)*100. Errors shown as ± values are 4 percent of calculated ages.
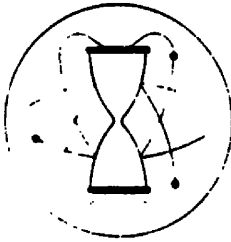
KRUEGER ENTERPRISES, INC.
GEOCHRON LABORATORIES DIVISION

24 BLACKSTONE STREET • CAMBRIDGE, MA. 02139 • (617)-876-3691

POTASSIUM–ARGON AGE DETERMINATION   REPORT OF ANALYTICAL WORK

Our Sample No.   F-6753   Date Received: 12/22/83

Your Reference: Letter of 12/19/83   Date Reported: 2/10/84

Submitted by: NORANDA Exploration, Inc.
                 2436 W. Central Ave.
                 Missoula, MT   59801
                 Attn: Carl Hering

Sample Description & Locality: Sample #IC-1019-5, porphyritic rhyolite.

Material Analyzed: Sanidine concentrate, -80/+200 mesh., Treated with
                      dilute HF and HNO_3 to remove alterations.

Ar^{40*}/K^{40} = .001164   AGE =   19.8 +/- 0.8   M.Y.

Argon Analyses:

Ar^{40*}, ppm.	$Ar^{40*}/$ Total Ar^{40}	Ave. Ar^{40*}, ppm.
.007067	.396	.007143
.007219	.534	

Potassium Analyses:

% K	Ave. %K	K^{40}, ppm
5.091	5.032	6.139
4.973		

Constants Used:

λ_β = 4.72 x 10^{-10}/ year

λ_e = 0.585 x 10^{-10}/ year

K^{40}/K = 1.22 x 10^{-4} g./g.

$$AGE = \frac{1}{\lambda_e + \lambda_\beta} \ln\left[\frac{\lambda_\beta + \lambda_e}{\lambda_e} \times \frac{Ar^{40*}}{K^{40}} + 1\right]$$

Note: Ar^{40*} refers to radiogenic Ar^{40}.
       M.Y. refers to millions of years.

KRUEGER ENTERPRISES, INC.
GEOCHRON LABORATORIES DIVISION

24 BLACKSTONE STREET • CAMBRIDGE, MA 02139 • (617) 876-3691

POTASSIUM–ARGON AGE DETERMINATION　　　　　**REPORT OF ANALYTICAL WORK**

Our Sample No.　M-6754　　　　　　　　Date Received: 12/22/83

Your Reference:　Letter of 12/19/83　　　　Date Reported:　2/10/84

Submitted by:　　NORANDA Exploration, Inc.
　　　　　　　　2436 W. Central Ave.
　　　　　　　　Missoula, MT　59801
　　　　　　　　Attn: Carl Hering

Sample Description & Locality:　Sample #IC-ZC-423, sericite/clay cemented
　　　　　　　　　　　　　　　gouge with sphalerite and galena clots.

Material Analyzed:　　Sericite concentrate, -80/+200 mesh.

$Ar^{40*}/K^{40} = .001290$　　　　　　　　　**AGE =** 21.9 +/- 0.9　M.Y.

Argon Analyses:

Ar^{40*}, ppm.	$Ar^{40*}/$ Total Ar^{40}	Ave. Ar^{40*}, ppm.
.007630	.681	.007854
.008078	.603	

Potassium Analyses:

% K	Ave. %K	K^{40}, ppm
5.052	4.990	6.087
4.927		

Constants Used:

$\lambda_\beta = 4.72 \times 10^{-10}$ / year
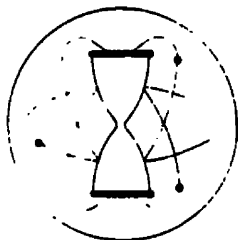
$\lambda_e = 0.585 \times 10^{-10}$ / year

$K^{40}/K = 1.22 \times 10^{-4}$ g./g.

$$AGE = \frac{1}{\lambda_e + \lambda_\beta} \ln\left[\frac{\lambda_\beta + \lambda_e}{\lambda_e} \times \frac{Ar^{40*}}{K^{40}} + 1\right]$$

Note:　Ar^{40*} refers to radiogenic Ar^{40}.
　　　　M.Y. refers to millions of years.

APPENDIX C. Fluid Inclusion Data

Description of analyzed surface samples
(locations given on Plate 2)

IC-40   - vitreous quartz associated with 7cm quartz-tourmaline breccia dike.
    - quartz contains abundant (>90%) Type II inclusions with little to no liquid phase present at room conditions, and some Type I inclusions.
    - many Type I inclusions believed to be of primary origin based on their large sizes and isolated distribution.

1018-4 - 1.5mm quartz-pyrite veinlet in quartz-sericite altered stockwork breccia. Pyrite is finely dispersed withing quartz along vein margins.
    - quartz contains abundant Type I, Type II, and Type III inclusions of unknown origin.

Descriptions of analyzed core samples
(sample prefix designates hole   and suffix indicates depth)

1C-29 - Silicified and sericitized breccia comprised of extremely fractured irregular quartz fragments cut by black, hairline quartz microveinlets.
    - quartz fragments are inclusion rich; most of which are secondary or of unknown origin. Type II inclusions are more abundant and generally larger than Type I inclusions.

1C-32 - 7mm sphalerite-clay healed drussy quartz vein in quartz sericite altered volcanics.
    - quartz contains abundant Type I, Type II and possible Type III inclusions, mostly of unknown origin. Type II inclusions are usually to small for use in heating/freezing tests.

1C-108.5 - 1-2mm quartz-toumaline-sphalerite-pyrite veinlet offset by
    quartz-pyrite microveinlet. Wall rocks are
    quartz-sericite-tourmaline altered.
        - quartz base-metal vein contains abundant Type II and some
    Type I inclusions of unknown origin. Type III inclusions are rare.
        - late quartz-pyrite microveinlet contains only Type I
    inclusions.

2C-199.8 - 1mm quartz-tourmaline-pyrite-sphalerite-chalcopyrite veinlet
    in quartz-sericite-pyrite altered volcanics. Veinlet has 1cm
    tourmalinized alteration selvage.
        - abundant Type I and Type II inclusions of unknown origin and
    minor Type III inclusions.

Heating/Freezing Results

Th (°C)

Th (°C)	IC-40	1018-4	IC-29	IC-32	EARLY IC-108.5	LATE IC-108.5	2C-199.8
~200	1		1				
			1				
			3			2	
	6		1		3	2	2
	10			1	2	1	2
300	3	2		1	3		3
	1	2	5	1	5.		
		1		2	3		6
		4	2	2	4		8
		4		3	8		10
400		2		1			4
		1					2
		1					
500					1		
>550		2					2

Salinity

Salinity	IC-40	1018-4	IC-29	IC-32	EARLY IC-108.5	LATE IC-108.5	2C-199.8
0	3 2		4 2	1	2 2		2 2
	1			1			
		2 2					
10			1		1		1
	1	1					
	2				1		4 1
20							
30					1		1
		4					
40		1					1
		2					
50							

Th= homogenization temperature
Salinity given in wt.% NaCl equivalent